EPA-450/4-88-006a
April 1988

A Dispersion Model For Elevated Dense Gas Jet Chemical Releases

Volume I.

U.S. ENVIRONMENTAL PROTECTION AGENCY
Office of Air and Radiation
Office of Air Quality Planning and Standards
Research Triangle Park, North Carolina 27711

DISCLAIMER

This report has been reviewed by the Office of Air Quality Planning and Standards, U.S. Environmental Protection Agency, and approved for publication as received from Dr. Jerry Havens. Approval does not signify that the contents necessarily reflect the views and policies of the U. S. Environmental Protection Agency, nor does mention of trade names or commercial products constitute endorsement or recommendation for use. Copies of this report are available from the National Technical Information Service (NTIS).

ACKNOWLEDGEMENTS

The elevated dense gas jet model incorporates methodology published by Ooms and his colleagues at the Technological University Delft, The Netherlands, along with the DEGADIS dense gas dispersion model developed at the University of Arkansas. Tom Spicer, my coauthor of DEGADIS, contributed to the development and was responsible for the modifications to DEGADIS required for interfacing with Ooms' model.

Jerry Havens

PREFACE

This version of the elevated dense gas dispersion model, Ooms/DEGADIS, has been developed by Dr. Jerry Havens and Dr. Tom Spicer of the University of Arkansas with the support of funding from the United States Environmental Protection Agency (EPA). It represents intermediate development of a dense gas modeling package which is undergoing further refinement through additional EPA support. While this model has not been extensively tested against field data, and is subject to specific limitations and uncertainties, the EPA is making it publicly available through the National Technical Information Service (NTIS) as an interim research tool pending further model evaluation and development.

The Ooms/DEGADIS model has been written in FORTRAN with specific intent for compilation and execution on a Digital Equipment Corporation VAX computer. Implementation of this model on any other computer system may be attempted at the risk of the user. Considerations for such implementation, however, are discussed in Appendix B of Volume II.

To facilitate dissemination of the model, it is being provided on two PC-compatible diskettes. The model should be uploaded via modem from a PC terminal to a host VAX computer, and several files must then be renamed prior to compilation and execution. Specific information on this process is contained in the file AAREADME.TXT. Print this file and the compilation batch file, BUILD.COM, prior to attempting compilation.

It is the concern of the EPA that this model be applied only within the framework of its intended use. To this end the user is referred to the specific recommendations in Volume I, Section VII for model application. These recommendations take advantage of the fact that, in this version of the Ooms/DEGADIS model, the portion of the model adapted from Ooms and his colleagues can be executed as a standalone model, as can the DEGADIS portion. To begin any particular simulation, it is recommended that the Ooms portion of the model be executed by itself.

This can be accomplished by setting the input variable <TEND> equal to 1. If the output from this simulation predicts that the plume will touch down less than 1 kilometer from the source, the complete Ooms/DEGADIS model may be appropriately applied (set <TEND> equal to zero or greater). If the plume is not predicted to touch down within 1 kilometer, this model should not be used.

VOLUME I

TABLE OF CONTENTS

LIST OF FIGURES

LIST OF TABLES

LIST OF SYMBOLS

NOTE: This list of symbols is divided into numbered sections corresponding to the sections of this report.

II. Characterizing Gas Density Effects on Dispersion

D	diameter of release (m)
g	gravitational acceleration (m/s)
H	characteristic height (depth) of release (m)
H_L	total layer depth in DEGADIS model (m)
k	von Karman's constant, 0.35
L_B	buoyancy length scale (m)
M_a	mass of air (kg)
Q	volumetric release rate (m^3/s)
R	radius of jet (m)
Ri_c	release Richardson number
Ri_*	Richardson number in Equation (V.78)
u	ambient (wind) velocity (m/s)
u_L	average transport velocity associated with H_L (m/s)
u_*	friction velocity (m/s)
V	jet velocity (m/s)
x	distance along jet axis (m)

II. Characterizing Gas Density Effects on Dispersion (symbols concluded)

ρ_a density of air (kg/m^3)

ρ_e density of released gas (kg/m^3)

ρ_L vertically averaged layer density (kg/m^3)

δ_L empirical constant (2.15) in Equation (V.53)

α constant in power law wind profile

ϕ density stratification effect function in Equation (V.76)

III. Description of the Ooms Model

b_j	characteristic plume width (radius = $b_j\sqrt{2}$), m
c	local concentration, kg/m^3
c_{jo}	concentration of jet at exit, kg/m^3
c^*	concentration on plume axis, kg/m^3
c_d	drag coefficient, 0.3
C_p	local heat capacity of plume, joule/kg K
C_{pa}	heat capacity of air, joule/kg K
C_{pj}	heat capacity of jet at exit, joule/kg K
g	gravitational acceleration, m/s^2
P	atmospheric pressure, newtons
r	radial distance to jet/plume axis, m
R	ideal gas law constant, 8314 joules/kg
s	distance along plume axis, m
u	local velocity in direction of plume axis, m/s
u_a	wind velocity, m/s
u*	plume excess velocity at plume axis, $u(r=0) - u_a\cos\theta$, m/s
u'	entrainment velocity due to atmospheric turbulence, m/s
T	local temperature of plume, K
T_a	temperature of air, K
T_{jo}	temperature of jet at exit, K
T'	reference temperature (T_a at jet exit elevation)
x	horizontal coordinate, m
y	vertical coordinate, m

III. Description of the Ooms Model (symbols concluded)

α_1	jet entrainment coefficient
α_2	line thermal entrainment coefficient
α_3	atmospheric turbulence entrainment coefficient
θ	angle between plume axis and horizontal, radians
λ	turbulence Schmidt number, 1.16
ρ	local density, kg/m^3
ρ_a	air density, kg/m^3
ρ'_a	density of air at elevation of jet exit
ρ^*	plume excess density at plume axis, $\rho(r=0) - \rho_a$, kg/m^3
μ	local molecular weight of plume, kg/kg mol
μ_j	molecular weight of jet at exit, kg/kg mol
μ_a	molecular weight of air, 28.9 kg/kg mol

a_v empirical constant (1.3) in Equations (V.6) and (V.27)

B_{EFF} effective width of gas plume (m)

B'_i local half width of source seen by observer i (m)

b half width of horizontally homogeneous central section of gas plume (m)

b_v empirical constant (1.2) in Equations (V.8) and (V.28)

C_E constant (1.15) in density intrusion (spreading) relation

C_p heat capacity (J/kg K)

C_{p_a} heat capacity of air (J/kg K)

C_{p_c} heat capacity of contaminant (J/kg K)

C_{p_w} heat capacity of water (liquid phase) (J/kg K)

c concentration (kg/m^3)

c_c centerline, ground-level concentration (kg/m^3)

$c_{c,L}$ vertically averaged layer concentration (kg/m^3)

c_f friction coefficient

c'_c centerline, ground-level concentration corrected for x-direction dispersion (kg/m^3)

D source diameter (m)

D_h added enthalpy (J/kg)

$\mathcal{D}$ diffusivity (m^2/s)

d_v empirical constant (0.64) in Equations (V.4) and (V.12)

E plume strength (kg/s)

E(t) contaminant primary source rate (kg contaminant/s)

e_v empirical constant (20.) in Equations (V.5) and (V.15)

F overall mass transfer coefficient (kg/m^2 s)

V. Description of the DEGADIS Model (symbols continued)

F_f mass transfer coefficient due to forced convection (kg/m^2 s)

F_n mass transfer coefficient due to natural convection (kg/m^2 s)

Gr Grashoff number

g acceleration of gravity (m/s^2)

H height or depth of density intrusion or cloud (m)

H_a ambient absolute humidity (kg water/kg dry air)

H_{EFF} effective cloud depth (m)

H_h height of head in density-driven flow (m)

H_L total layer depth (m)

H_t height of tail in density-driven flow (m)

H_1 average depth of gravity current head (m)

H_4 depth of inward internal flow in a gravity current head (m)

h enthalpy of source blanket (J/kg)

h_a enthalpy of ambient humid air (J/kg)

h_E enthalpy associated with primary source mass rate (J/kg)

h_f heat transfer coefficient due to forced convection (J/m^2 s K)

h_L enthalpy of vertically averaged layer (J/kg)

h_n heat transfer coefficient due to natural convection (J/m^2 s K)

h_0 overall heat transfer coefficient (J/m^2 s K)

h_p enthalpy of primary source (J/kg)

h_w enthalpy associated with mass flux of water from surface (J/kg)

K_0 constant in Equation (V.96) ($m^{1-\gamma_1}$)

V. Description of the DEGADIS Model (symbols continued)

K_y	horizontal turbulent diffusivity (m^2/s)
K_z	vertical turbulent diffusivity (m^2/s)
k	von Karman's constant, 0.35
k_1	constant in Equation (V.13)
k_2	constant in Equation (V.14)
L	source length (m)
M	total cloud mass (kg)
M_a	total mass of air in the cloud (kg)
M_c	total mass of contaminant in the cloud (kg)
M_i	initial cloud mass (kg)
MW	molecular weight
$\dot{M}_a$	mass rate of air entrainment into the cloud (kg/s)
$\dot{M}_{w,s}$	mass rate of water transfer to the cloud from the water surface under the source (kg/s)
N	number of observers
Nu	Nusselt number
P	cloud momentum (kg m/s)
P_h	momentum of head in density-driven flow (kg m/s)
P_t	momentum of tail in density-driven flow (kg m/s)
P_v	virtual momentum due to acceleration reaction (kg m/s)
Pr	Prandtl number
p	atmospheric pressure (atm)
$p_{w,c}$	partial pressure of water in the cloud (atm)
$p^*_{w,s}$	vapor pressure of water at the surface temperature (atm)
Q	volumetric release rate (m^3/s)

V. Description of the DEGADIS Model (symbols continued)

Q_E	source mass flux (kg/m^2 s)
Q_e	volumetric entrainment flux (m/s)
Q_1	flux of ambient fluid into front of gravity current head (m/s)
$\dot{Q}_s$	rate of heat transfer from the surface (J/s)
Q_*	atmospheric takeup flux (kg/m^2 s)
Q_{*max}	maximum atmospheric takeup flux of contaminant (kg/m^2 s)
q_s	surface heat flux (J/m^2 s)
R	gas source cloud radius (m)
R_h	inner radius of head in density-drive flow (m)
R_m	value of R when ($\pi R^2 Q_*$) is a maximum (m)
R_{max}	maximum radius of the cloud (m)
R_p	primary source radius (m)
Ri_f	Richardson number associated with the front velocity, Equation (V.11)
Ri_T	Richardson number associated with temperature differences, Equation (V.88)
Ri'_*	Richardson number associated with density differences corrected for convective scale velocity
Ri_*	Richardson number associated with density differences, Equation (V.78)
Sc	Schmidt number
Sh	Sherwood number
St_H	Stanton number for heat transfer
St_M	Stanton number for mass transfer
S_y	horizontal concentration scaling parameter (m)
S_z	vertical concentration scaling parameter (m)
S_{z0}	S_z at the downwind edge of the source (x = L/2) (m)

S_{z0_m} value of S_{z0} when $(\pi R^2 Q_*)$ is a maximum (m)

T temperature associated with source blanket enthalpy (K)

$T_{c,L}$ temperature associated with layer-averaged enthalpy (K)

T_s surface temperature (K)

t time (s)

t_s specified time (s)

t_{dn_i} time when observer i encounters downwind edge (s)

t_{up_i} time when observer i encounters upwind edge (s)

u_a ambient average velocity (m/s)

u_e horizontal or frontal entrainment velocity (m/s)

u_{EFF} effective cloud advection velocity (m/s)

u_f cloud front velocity (m/s)

u_i velocity of observer i (m/s)

u_L average transport velocity associated with H_L (m/s)

u_x wind velocity, along x-direction (m/s)

u_0 wind velocity measured at $z = z_0$ (m/s)

u_3 internal flow out of gravity current head (m/s)

u_4 internal flow into gravity current head (m/s)

u_* friction velocity (m/s)

$\bar{u}$ characteristic average velocity (m/s)

V_H heat transfer velocity (0.0125 m/s) in Equation (V.38) (m/s)

w_a mass fraction of air

w_c mass fraction of contaminant

$w_{c,p}$ mass fraction of contaminant in primary source

w_e vertical entrainment velocity associated with H_L (m/s)

V. Description of the DEGADIS Model (symbols continued)

w_*	convective scale velocity (m/s)
w'_e	entrainment velocity associated with H_{EFF} (m/s)
$x_i(t)$	x position of observer i at time t (m)
x_{pi}	position of puff center due to observer i (m)
x_t	downwind distance where gravity spreading terminates (m)
x_v	virtual point source distance (m)
x_{dn_i}	x position of downwind edge of source for observer i
x_{up_i}	x position of upwind edge of source for observer i
x,y,z	Cartesian coordinates (m)
x_0	downwind edge of the gas source (m)
z_R	surface roughness (m)
z_0	reference height in wind velocity profile specification (m)
α	constant in power law wind profile
β	constant in σ_y correlation in Equation (V.97)
Γ	gamma function
γ	ratio of $(\rho - \rho_a)/c_c$
γ_1	constant in Equation (V.96)
Δ	ratio of $(\rho - \rho_a)/\rho$
ΔT	temperature driving force (K) $(T_s - T_{c,L})$ or $(T_s - T)$
Δ'	ratio of $(\rho - \rho_a)/\rho_a$
δ	constant in σ_y correlation in Equation (V.97)
δ_L	empirical constant (2.15) in Equation (V.53)
δ_v	constant (0.20) in Equation (V.25)
ϵ	frontal entrainment coefficient (0.59) in Equation (V.33)

V. Description of the DEGADIS Model (symbols concluded)

ζ	collection of terms defined by Equation (V.62) ($m^{-1/(1+\alpha)}$)
λ	Monin-Obukhov length (m)
μ	viscosity (kg/m s)
ρ	density of gas-air mixture (kg/m^3)
ρ_a	ambient density (kg/m^3)
ρ_c	cloud density (kg/m^3)
ρ_L	vertically averaged layer density (kg/m^3)
ρ_0	density of contaminant's saturated vapor at T_0 (kg/m^3)
σ_x	Pasquill-Gifford x-direction dispersion coefficient (m)
σ_y	Pasquill-Gifford y-direction dispersion coefficient (m)
σ_z	Pasquill-Gifford z-direction dispersion coefficient (m)
ϕ	function describing influence of stable density stratification on vertical diffusion, Equation (V.76)
$\hat{\phi}$	integrated source entrainment function
ψ	logarithmic velocity profile correction function

Summary

A mathematical model was developed for estimating ambient air concentrations downwind of elevated, denser-than-air gas jet-type releases. Ooms' model is used to predict the trajectory and dilution, to ground contact, of a denser-than-air jet/plume. The output of Ooms' model interfaces with the DEGADIS dense gas dispersion model to predict the ensuing ground level dispersion. The model incorporates momentum and heat transfer important to turbulent diffusion in the surface layer of the atmospheric boundary layer and provides for:

- inputting data directly from external files
- treatment of ground-level or elevated sources
- estimation of maximum concentrations at fixed sites
- iteration over discrete meteorological conditions
- estimation of concentration-time history at fixed sites.

This report and the accompanying User's Guide (Volume II):

- document the theoretical basis of the model
- discuss its applicability and limitations
- discuss criteria for estimating the importance of gas density effects on a jet release from an elevated source
- define and describe all input variables and provide appropriate guidance for their specification
- identify and describe all output files and provide appropriate guidance for their interpretation
- provide user instructions for executing the code
- illustrate the model usage with example applications.

I. INTRODUCTION

Episodic releases of hazardous chemical gases in chemical process pressure relief operations may pose significant hazards to public health, and methods are required for assessing their consequences. Conventional air pollutant dispersion models may not be applicable to such releases, particularly when the gases released are denser than air. Although there has been considerable recent development of dense gas dispersion models, such models have only been demonstrated for predicting dispersion of gases released at ground level on flat, obstacle-free terrain. The DEGADIS model (Havens and Spicer, 1985) was developed for simulating dispersion of zero momentum, ground-level, heavy gas releases. DEGADIS describes the dispersion processes which accompany the ensuing gravity-driven flow and entrainment of the gas into the atmospheric boundary layer. DEGADIS has been verified by comparison with a wide range of laboratory and field-scale heavy gas release/dispersion data. However, DEGADIS makes no provision for processes which occur in high velocity releases, as from pressure relief valves.

Ooms, Mahieu, and Zelis (1974) reported a mathematical model for estimating trajectory and dilution of dense gas vent jets. The model comprises simplified balance equations for mass, momentum, and energy, with Gaussian similarity profiles for velocity, density, and concentration in the jet.

The purpose of this work was to evaluate Ooms' model for prediction of the trajectory (to ground contact) and dilution of elevated dense gas jet releases, and to provide for interfacing Ooms' model with DEGADIS. The Ooms model can be used to predict the downwind distance where the dense jet/plume falls to ground level and the plume concentration at ground contact, and the Ooms model output can be used as initial (input) conditions to DEGADIS for prediction of the ensuing ground-level plume dispersion.

II. CHARACTERIZING GAS DENSITY EFFECTS ON ATMOSPHERIC DISPERSION

Atmospheric dispersion of gases released with low momentum may be characterized by three more-or-less distinct fluid flow regimes:

buoyancy-dominated • stably stratified • passive dispersion

The three regimes, which may be present to different degrees depending on the rate and (characteristic) dimensions of the release, the gas density, and the characteristics of the atmospheric flow, must be accounted for if a model is to be generally applicable. Estimation of atmospheric dispersion when the gas is released at high momentum (velocity) may require consideration of (additional) air entrainment due to the accompanying jetting effect.

In rapid releases of large quantities of dense gas (with little initial momentum) a cloud having similar vertical and horizontal dimensions may form. In this "buoyancy-dominated regime", (gravity-induced) slumping and lateral spreading motion ensues until the kinetic energy of the buoyancy-driven flow is dissipated. The gravity-induced flow may effect mixing (primarily at the advancing vapor cloud front) which can be an important determinant of the shape and extent of the gas cloud. After the buoyancy-induced kinetic energy is dissipated, the dispersion process which follows can be described as a "stably stratified" plume (or cloud) embedded in the mean wind flow. The density stratification present in this regime, which can be much stronger than that occurring naturally in the atmospheric boundary layer, tends to damp turbulence and reduce vertical mixing. As the dispersion proceeds, the stable stratification due to the dense gas decreases until the dispersion process can be represented as a neutrally buoyant plume (or cloud) in the mean wind flow. This final regime of "passive" dispersion (by pre-existing turbulence) in the atmosphere can be predicted using trace contaminant dispersion theory. For low-momentum dense gas releases at ground level on uniform, level terrain with unobstructed atmospheric flow, the buoyancy-dominated, stably-stratified, and passive dispersion regimes can be modeled with DEGADIS (Havens and Spicer, 1985).

Based on water tunnel experiments reported by Britter (1980), Havens and Spicer (1985) suggested criteria for determining the importance of each of the three flow regimes described above for zero-initial-momentum, ground-level releases. In Britter's experiment brine was released at floor level into a water tunnel flow, and the lateral and upwind extent of the brine/water plume was recorded as a function of the buoyancy length scale

$$L_B = Qg(\rho_E - \rho_a)/(\rho_E u^3)$$

where Q was the volumetric (brine) emission rate and u was the water-tunnel flow velocity. Britter's data indicated releases were passive from the source when $L_B/D \lesssim 0.005$ and were dominated by the negative buoyancy dispersion regime when $L_B/D \gtrsim 0.1$. The following Release Richardson number criteria, based on these observations, were suggested:

If $Ri_c \gtrsim 30$	negative buoyancy-dominated	
If $1 \lesssim Ri_c \lesssim 30$	stably stratified shear flow	(II-1)
If $Ri_c \lesssim 1$	passive dispersion	

where $Ri_c = g(\rho_E - \rho_a)H/(\rho_a u_*^2)$. The reported values reflect the ratio $(u/u_*) = 16$ for Britter's water-tunnel flow, and the length scale corresponding to the depth of the layer was approximated by $H = Q/uD$.

Releases with initial momentum may require consideration of jet effects. A release may be considered importantly affected by jet effects if the rate of air entrainment due to jetting action dominates that due to other air entrainment mechanisms.

In the negative buoyancy-dominated regime, the ambient flow does not importantly affect the rate of (nonjet) air entrainment. For this case, the relative importance of jet effects can be evaluated using the criterion based on Britter's data (with the release velocity V used in place of the ambient velocity in the buoyancy length scale). It follows that jet effects dominate the negative buoyancy regime when

$$\left[\frac{V}{u_*}\right]^2 \gtrsim 10\ Ri_c \qquad \text{(II-2)}$$

This criterion has the characteristic that as the density of the released fluid increases, the release is less readily dominated by jet effects (since the rate of air entrainment would increase in the absence

of the jet effects due to the entrainment associated with the gravity front).

The air entrainment into a turbulent free jet can be estimated as suggested by Wheatley (1986).

$$\frac{dM_a}{dx} = \left[\frac{0.159}{2}\right]\left[\frac{2\pi R}{2}\right] V \rho_a \qquad \text{(II-3)}$$

The rate of (vertical) air entrainment (per unit width) for the stably stratified shear flow and passive dispersion regimes predicted by DEGADIS is

$$\frac{d}{dx}(\rho_L u_L H_L) = \frac{\rho_a \delta_L k u_* (1 + \alpha)}{\phi(Ri_*)} \qquad \text{(II-4)}$$

where $\phi(Ri_*) = 0.88 + 0.099\ Ri_*$. Using an effective width of $2\pi R$, a typical value of $\alpha = 0.2$, $\delta_L = 2.1$, $k = 0.35$, and $(u/u_*) = 30$ (typical of atmospheric boundary layers), the above equations can be combined to show that jet effects dominate the stably-stratified flow regime when

$$\frac{V}{u} \gtrsim 16/(19 + Ri_c) \qquad \text{(II-5)}$$

This criterion has the characteristic that as the density of the released fluid increases, the release is more readily dominated by jet effects (since the rate of air entrainment would decrease in the absence of the jet effects). When $Ri_c \lesssim 1$ the criterion indicates that jet effects dominate the passive dispersion regime when $(V/u) \gtrsim 0.8$, which is consistent with the criterion suggested by Cude (1974) and Wheatley (1986).

Summarizing, the following procedure is suggested for determining which dispersion regime is dominant from the start of a release:

(1) Calculate $Ri_c = g(\rho_E - \rho_a)H/(\rho_a u_*^2)$.

(2) Determine the dominant nonjet dispersion regime in the absence of a jet using Equation (II-1).

(3) Determine if ground-level jet effects dominate the dominant nonjet regime determined from (2) using the relationships summarized in Table II.1.

TABLE II.1
CRITERIA FOR DETERMINING WHETHER JET EFFECTS
DOMINATE A GROUND-LEVEL RELEASE

Ground-level jet effects dominate:	
Negative buoyancy-dominated regime when	$\left(\frac{V}{u_*}\right)^2 \geq 10\ Ri_c$
Stably stratified shear flow regime when	$V/u \geq 16/(19 + Ri_c)$
Passive dispersion phase when	$V/u \geq 0.8$

III. DESCRIPTION OF THE OOMS MODEL

Ooms, Mahieu, and Zelis' (1974) model comprises simplified balance equations for mass and momentum to describe the jet illustrated in Figure III.1.

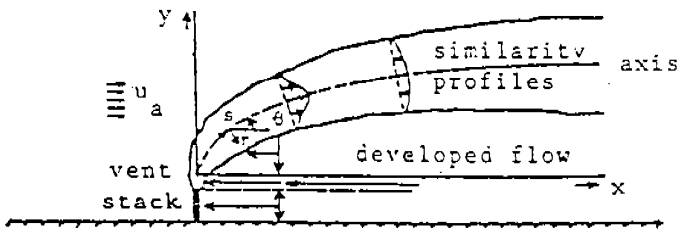

Figure III.1. Schematic diagram of Ooms' model.

Gaussian similarity profiles for velocity, density, and concentration are assumed to apply in the developed jet:

$$u(s,r,\theta) = u_a \cos\theta + u^*(s)\, e^{-r^2/b_j^2(s)} \qquad \text{(III.1)}$$

$$\rho(s,r,\theta) = \rho_a + \rho^*(s)\, e^{-r^2/\lambda^2 b_j^2(s)} \qquad \text{(III.2)}$$

$$c(s,r,\theta) = c^*(s)\, e^{-r^2/\lambda^2 b_j^2(s)} \qquad \text{(III.3)}$$

Balance equations for mass and horizontal and vertical momentum are:

Component Mass

$$\frac{d}{ds}\int_0^{b_j\sqrt{2}} 2\pi r c u dr = 0 \qquad \text{(III.4)}$$

Overall Mass

$$\frac{d}{ds}\int_0^{b_j\sqrt{2}} 2\pi r \rho u dr = 2\pi b_j \rho_a \left\{ \alpha_1 |u^*(s)| + \alpha_2 u_a |\sin\theta| \cos\theta + \alpha_3 u' \right\} \qquad \text{(III.5)}$$

Horizontal (x-direction) Momentum

$$\frac{d}{ds}\int_0^{b_j\sqrt{2}} 2\pi r \rho u^2 \cos\theta \, dr = 2\pi b_j \rho_a u_a \left\{ \alpha_1 |u^*(s)| + \alpha_2 u_a |\sin\theta| \cos\theta + \alpha_3 u' \right\} + c_d \pi b_j \rho_a u_a^2 |\sin^3\theta| \qquad \text{(III.6)}$$

Vertical (y-direction) Momentum

$$\frac{d}{ds}\int_0^{b_j\sqrt{2}} 2\pi r \rho u^2 \sin\theta \, dr = \int_0^{b_j\sqrt{2}} 2\pi r g(\rho_a - \rho) dr - \text{sign}(\theta)\, c_d \pi b_j \rho_a u^2 \sin^2\theta \cos\theta \qquad \text{(III.7)}$$

Energy

$$\frac{d}{ds}\int_0^{b_j\sqrt{2}} 2\pi r \rho u C_p (T - T') dr = 2\pi b_j \rho_a C_{pa} (T_a - T') \left\{ \alpha_1 |u^*(s)| + \alpha_2 u_a |\sin\theta| \cos\theta + \alpha_3 u' \right\} \qquad \text{(III.8)}$$

The temperatures of the plume and air are calculated from the ideal gas law, with the plume (gas-air mixture) molecular weight and heat capacity estimated using ideal gas mixing relations:

$$T = \frac{P\mu}{R\rho} \quad \text{and} \quad T_a = \frac{P\mu_a}{R\rho_a} \tag{III.9}$$

$$\mu = \mu_j \frac{cT}{c_{jo}T_{jo}} + \mu_a \left(1 - \frac{cT}{c_{jo}T_{jo}} \right) \tag{III.10}$$

$$\mu C_p = \mu_j C_{pj} \frac{cT}{c_{jo}T_{jo}} + \mu_a C_{pa} \left(1 - \frac{cT}{c_{jo}T_{jo}} \right) \tag{III.11}$$

Substitution of Equations (III.9-III.11) in the energy balance equation (III.8) gives

$$\frac{d}{ds} \int_0^{b_j\sqrt{2}} 2\pi r u \frac{\mu C_p}{\mu_a C_{pa}} \left\{ 1 - \frac{\rho}{\rho_a} \left[1 + \frac{c\rho_{jo}}{c_{jo}\rho} \left(\frac{\mu_a}{\mu_{jo}} - 1 \right) \right] \right\} dr =$$

$$2\pi b_j \left(1 - \frac{\rho_a}{\rho'_a} \right) \left\{ \alpha_1 |u^*(s)| + \alpha_2 u_a |\sin\theta| \cos\theta + \alpha_3 u' \right\} \tag{III.12}$$

Approximating the product of plume molecular weight and heat capacity using the relation (following Ooms et al., 1974)

$$\frac{\mu C_p}{\mu_a C_{pa}} = \frac{1}{2} \left(1 + \frac{\mu_{jo} C_{pj}}{\mu_a C_{pa}} \right) , \tag{III.13}$$

and utilizing the similarity profiles and the ideal gas equation of state, the balance equations were integrated over the radius of the plume to give a set of ordinary differential equations:

$$\begin{bmatrix} A_{11} & A_{12} & A_{13} & A_{14} & A_{15} \\ A_{21} & A_{22} & A_{23} & A_{24} & A_{25} \\ A_{31} & A_{32} & A_{33} & A_{34} & A_{35} \\ A_{41} & A_{42} & A_{43} & A_{44} & A_{45} \\ A_{51} & A_{52} & A_{53} & A_{54} & A_{55} \end{bmatrix} \begin{bmatrix} dc^*/ds \\ db/ds \\ du^*/ds \\ d\theta/ds \\ d\rho^*/ds \end{bmatrix} = \begin{bmatrix} B_{j1} \\ B_{j2} \\ B_{j3} \\ B_{j4} \\ B_{j5} \end{bmatrix} \qquad \text{(III.14)}$$

where

$$A_{11} = b(k_1 u_a \cos\theta + k_2 u^*)$$

$$A_{12} = 2c^*(k_1 u_a \cos\theta + k_2 u^*)$$

$$A_{13} = k_2 c^* b$$

$$A_{14} = -k_1 u_a c^* b \sin\theta$$

$$A_{15} = 0$$

...

$$A_{21} = 0$$

$$A_{22} = 2(2u_a \cos\theta + k_3 u^* + k_4 \rho^* u_a \cos\theta/\rho_a + k_5 \rho^* u^*/\rho_a)$$

$$A_{23} = b(k_3 + k_5 \rho^*/\rho_a)$$

$$A_{24} = b(-2u_a \sin\theta - k_4 \rho^* u_a \sin\theta/\rho_a)$$

$$A_{25} = b(k_4 u_a \cos\theta + k_5 u^*)/\rho_a$$

...

$$A_{31} = 0$$

$$A_{32} = 2u^* \cos\theta(k_6 u_a \cos\theta + k_7 u^* + \rho^*/\rho_a(k_8 u_a \cos\theta + k_9 u^*)) + u_a^2 \cos^3\theta(4 + 2k_4 \rho^*/\rho_a)$$

$$A_{33} = b \cos\theta(k_6 u_a \cos\theta + k_{10} u^* + \rho^*/\rho_a(k_8 u_a \cos\theta + k_{11} u^*))$$

$$A_{34} = b u_a \cos\theta \sin\theta(-6u_a \cos\theta - k_{12} u^* - k_{13} u_a \cos\theta \, \rho^*/\rho_a - k_{14} u^* \rho^*/\rho_a) - b u^{*2} \sin\theta(k_7 + k_9 \rho^*/\rho_a)$$

$$A_{35} = b(k_4 u_a^2 \cos^2\theta \cos\theta + k_8 u_a \cos\theta \, u^* \cos\theta + k_9 u^{*2} \cos\theta)/\rho_a$$

...

$$A_{41} = 0$$

$$A_{42} = 2\cos\theta\ \sin\theta(2u_a^2\cos\theta + k_6u_au^* + k_4u_a^2\cos\theta\ \rho^*/\rho_a + k_8u_au^*\rho^*/\rho_a) + 2\sin\theta(k_7u^{*2} + k_9u^{*2}\rho^*/\rho_a)$$

$$A_{43} = b\ \sin\theta(k_6u_a\cos\theta + k_{10}u^* + \rho^*/\rho_a(k_8u_a\cos\theta + k_{11}u^*))$$

$$A_{44} = bu_a^2\cos\theta(1-3\sin^2\theta)(2 + k_4\rho^*/\rho_a) + bk_7u^{*2}\cos\theta + b(\cos^2\theta-\sin^2\theta)u_au^*(k_6 + k_8\rho^*/\rho_a) + bk_9u^{*2}\cos\theta\ \rho^*/\rho_a$$

$$A_{45} = b(k_4u_a^2\cos^2\theta\ \sin\theta + k_8u^*\sin\theta\ \cos\theta\ u_a + k_9u^{*2}\sin\theta)/\rho_a$$

...

$$A_{51} = -k_{15}\text{group1 group4 } u_ab_j^2\cos\theta - k_{17}\text{group1 group4 } b_j^2u^*$$

$$A_{52} = 2b_j(u_a\text{group3 }\cos\theta - k_{15}u_a\cos\theta\ \rho^*/\rho' - k_{15}\text{group1 group4 } u_ac^*\cos\theta + k_{16}\text{group3 } u^* - k_{17}(u^*\rho^*/\rho' + \text{group1 group4 } c^*u^*)$$

$$A_{53} = b_j^2(k_{16}\text{group3} - k_{17}(\rho^*/\rho' + c^*\text{group1 group4})$$

$$A_{54} = -\sin\theta(\text{group3 } u_ab_j^2 - k_{15}\ b_j^2u_a\rho^*/\rho' - k_{15}\text{group1 group4 } b_j^2\ u_a^*c)$$

$$A_{55} = -k_{15}b_j^2u_a\cos\theta/\rho' - k_{17}b_j^2u^*/\rho'$$

...

$$B_1 = 0$$

$$B_2 = 2(\alpha_1|u^*| + \alpha_2u_a|\sin\theta|\cos\theta + \alpha_3u')$$

$$B_3 = 2u_a(\alpha_1|u^*| + \alpha_2u_a|\sin\theta|\cos\theta + \alpha_3u') + c_du_a^2|\sin^3\theta|$$

$$B_4 = -k_4b_jg\rho^*/\rho_a \pm c_du_a^2\sin^2\theta\ \cos\theta$$

$$B_5 = \text{rtside}/(\pi(\text{group2} + 1.))$$

and

μ_a = mol weight, air group1 = $\frac{\mu_a}{\mu} - 1$ group2 = $\frac{\mu_{jo}C_{pj}}{\mu_aC_{pa}}$

μ_j = mol weight, jet group3 = $1 - \frac{\rho_a}{\rho'}$ group4 = $\frac{\rho_j}{c^*\rho'}$

$k_1 = 0.772699$	$k_2 = 0.412442$	$k_3 = 0.864665$
$k_4 = 1.043144$	$k_5 = 0.556796$	$k_6 = 1.729329$
$k_7 = 0.490842$	$k_8 = 1.113593$	$k_9 = 0.363346$
$k_{10} = 0.981684$	$k_{11} = 0.726692$	$k_{12} = 3.458658$
$k_{13} = 3.129432$	$k_{14} = 0.227186$	$k_{15} = 0.521572$
$k_{16} = 0.432332$	$k_{17} = 0.278398$	

Initial conditions for Ooms' model were specified at the beginning of the "developed flow" region of the jet (Figure III.1). The trajectory of the jet to the developed flow region was calculated using wind-tunnel data correlations by Kamotani and Greber (1972). The differential equations were solved with the subroutine SIMUL and integrated using the subroutines RUNGE and HAMING, described by Carnahan, Luther, and Wilkes (1969).

The balance equations for mass and momentum incorporate empirical coefficients for estimating air entrainment. The coefficients α_1, α_2, and α_3 provide for entrainment as follows:

α_1 is the entrainment coefficient for a turbulent free jet. The value 0.057 was incorporated by Ooms, after Albertson, et al. (1950).

α_2 accounts for entrainment into the plume at a sufficiently long distance downwind of the vent where the velocity of the plume approaches the wind velocity. The value 0.5 was incorporated by Ooms, after Richards (1963).

α_3 accounts for entrainment due to atmospheric turbulence. Ooms suggested estimation of the entrainment velocity as $u' = (\epsilon b_j)^{1/3}$, with specification of ϵ (the eddy energy dissipation) as a function of height, wind velocity, and atmospheric stability. The eddy energy dissipation for a neutral atmosphere was recommended by Briggs (1969):

$\epsilon = 0.0677\ u_a/z\ (m^2/s^3)$ for $z < 300$ m

and for "unstable" and "stable" atmospheres by Kaimal et al. (1976):

$\epsilon = 0.004\ (m^2/s^3)$ for unstable atmospheres

$\epsilon = 0$ for stable atmospheres

The value 1.0 for α_3 was incorporated by Ooms, after Briggs (1969).

IV. EVALUATION OF THE OOMS MODEL

A series of simulations were made with the Ooms model to:

- compare the model predictions with wind tunnel dense gas jet trajectory and dilution data
- characterize the sensitivity of the model to the specification of entrainment coefficients α_1, α_2, and α_3

Table IV.1 shows the "typical" jet releases simulated.

TABLE IV.1
SPECIFICATION OF GAS RELEASE RATES FOR MODELING

Jet Diameter m	Jet Velocity m/s	Gas Release Rate kg/s
0.05 (~2 in)	30.6 (~100 ft/s)	0.24
0.2 (~8 in)	91.7 (~300 ft/s)	11.52
0.5 (~20 in)	213.9 (~700 ft/s)	168.0

Comparison with Wind Tunnel Test Data

Hoot, Meroney, and Peterka (1973) reported plume rise, downwind distance to plume touchdown, and dilution at touchdown for wind tunnel jet releases of Freon-12/air mixtures. The ranges of experimental variables studied were:

gas specific gravity (air = 1)	1.1 - 4.6
gas exit diameter, cm	0.32 and 0.64
gas exit height, cm	7.6 and 15.2
gas exit velocity/wind velocity ratio	2.5 - 25
wind (tunnel) velocity, m/s	0.23 and 0.46

Correlations (of the wind tunnel data) were presented for plume rise, distance to plume touchdown, and plume centerline concentration at ground contact, in a laminar crosswind:

Plume Rise

$$H = 1.32\ D\ [(u/u_a)(\rho/\rho_a)]^{1/3} Fr^{2/3}$$

Downwind Distance to Maximum Rise

$$\bar{X} = (D\ u\ /u_a)\ Fr^{\ 2}$$

Downwind Distance to Centerline Ground Contact

$$X = 0.56\ D\ \{(H/D)^3[(2 + H_s/H)^3 - 1]u_a/u\}^{1/2} Fr_h + \bar{X}$$

Centerline Concentration at Ground Contact

$$\chi = 3.1\ (Q/u_a D^2)\ [(2H + H_s)/D]^{-1.95}$$

where D = jet diameter (initial), m
Fr = Froude number, $u/[g\ D\ [(\rho-\rho_a)/\rho]^{1/2}$
Fr_h = "horizontal" Froude number, $u_a/[g\ D\ [(\rho-\rho_a)/\rho_a]^{1/2}$
H = maximum height of plume rise, m
H_s = exit height, m
Q = jet rate (initial), kg/s
u_a = wind velocity, m/s
u = jet velocity (initial), m/s
X = downwind distance to ground contact (centerline), m
$\bar{X}$ = downwind distance to maximum rise, m
ρ_a = ambient air density, kg/m^3
ρ = jet density (initial), kg/m^3
χ = jet centerline concentration, kg/m^3

Table IV.2 compares the Ooms model predictions for plume rise, downwind distance to ground contact, and concentration at ground contact with the results of Hoot et al.'s wind-tunnel data correlations for the "low diameter/low velocity", "typical diameter/typical velocity," and "high diameter/high velocity" cases (Table IV.1) in 3 and 6 m/s winds.

TABLE IV.2
COMPARISON OF OOMS MODEL PREDICTION WITH
HOOT ET AL.'S WIND-TUNNEL DATA CORRELATION

Gas Jet Density: 4.0 kg/m3 Gas Jet Elevation: 10 m

(Hoot et al. correlation / Ooms model prediction)

Maximum Height, m (3, 6 mps)		Distance to Ground Contact, m (3, 6 mps)		Centerline Concentration at Ground Contact $kg/m^3 \times 10^3$ (3, 6 mps)	
Low Diameter (0.05 m) / Low Velocity (30.6 m/s)					
3.0/2.2	2.4/1.6	150/140	375/325	1.3/1.9	0.8/1.2
Typical Diameter (0.2 m) / Typical Velocity (97.1 m/s)					
23.0/19.0	18.0/13.8	165/170	350/305	5.2/7.5	3.7/6.1
High Diameter (0.5 m) / High Velocity (213.9 m/s)					
97.0/79.0	77.0/61.0	320/415	650/705	5.6/7.6	4.3/6.2

The Ooms model predictions assumed a power law vertical velocity profile with the 3 and 6 m/s velocities at 10 m elevation and a power law wind profile constant 0.142. Since the wind tunnel correlations were for jets directed into a laminar crosswind, the jet model predictions shown in Table IV.2 were made with the entrainment coefficient accounting for atmospheric turbulence, α_3, set to zero.

The model predictions of maximum rise, distance to ground contact, and concentration at ground contact are in good agreement with predictions from the wind tunnel data correlations, considering the uncertainty in representing the (tunnel) wind profile.

Sensitivity to Entrainment Coefficient Specification

The model sensitivity to the entrainment coefficients α_1 and α_2 (with $\alpha_3 = 0$) was determined first. Specification of α_3 equal to zero

is equivalent to specifying stable stratification of the atmospheric flow (with zero turbulent entrainment). The model sensitivity to the coefficients α_1 and α_2 was determined by systematic variation around the values recommended by Ooms. All simulations were of heavy gas jets (exit density 4.0 kg/m^3) exiting vertically upward at 10 meters elevation. The predictions assumed a power law vertical velocity profile with the 3 and 6 m/s velocities at 10 m elevation and a power law wind profile constant 0.142. Table IV.3 shows the effect of individually varying the entrainment coefficients α_1 and α_2 by factors of two below and above the values recommended by Ooms, for the "low diameter/low velocity", "typical diameter/typical velocity," and "high diameter/high velocity" cases (Table IV.1) in 3 and 6 m/s winds.

The predictions of maximum rise and distance to ground contact are relatively insensitive to factor-of-four variation in the entrainment coefficient α_1 over the range of release conditions in Table IV.1. The predictions of concentration at ground contact are very insensitive to the same variation in α_1. The predictions of maximum rise and distance to ground contact are more sensitive to factor-of-four variation in the coefficient α_2, and the concentration at ground contact changes by factors of about 4, 6, and 10 for the high diameter/high velocity, typical diameter/typical velocity, and low diameter/ low velocity cases, respectively.

The model sensitivity to all three entrainment coefficients (α_1, α_2, and α_3) was also determined by systematic variation around the values recommended by Ooms. Again, all simulations were of heavy gas jets (exit density 4.0 kg/m^3) exiting vertically upward at 10 meters elevation, assuming a power law vertical velocity profile with the 3 and 6 m/s velocities at 10 m elevation and a power law wind profile constant 0.142. Table IV.4 shows the effect of individually varying the entrainment coefficients α_1, α_2, and α_3 by factors of two below and above the values recommended by Ooms, for the "low diameter/low velocity", "typical diameter/typical velocity," and "high diameter/high velocity" cases in 3 and 6 m/s winds.

Again, the predictions of maximum rise are relatively insensitive to factor-of-four variation in the entrainment coefficient α_1 over the

TABLE IV.3
SENSITIVITY OF OOMS MODEL PREDICTION TO
VARIATION OF ENTRAINMENT COEFFICIENTS α_1 and α_2
WITH NO ATMOSPHERIC TURBULENCE ENTRAINMENT

Gas Jet Density: 4.0 kg/m3 Gas Jet Elevation: 10 m

Entrainment Coefficients α_1	α_2	α_3	Maximum Height, m (3, 6 mps)		Distance to Ground Contact, m (3, 6 mps)		Centerline Concentration at Ground Contact kg/m^3 (3, 6 mps)	
Low Diameter (0.05 m) / Low Velocity (30.6 m/s)								
0.03	0.5	0.0	12.6	11.7	145	325	0.00190	0.00124
0.057	0.5	0.0	12.2	11.5	140	325	0.00192	0.00122
0.12	0.5	0.0	11.9	11.4	140	320	0.00185	0.00124
0.057	0.25	0.0	12.6	11.9	100	220	0.00522	0.00363
0.057	0.5	0.0	12.2	11.5	140	325	0.00192	0.00122
0.057	1.0	0.0	11.8	11.2	215	520	0.00062	0.00037
Typical Diameter (0.2 m) / Typical Velocity (97.1 m/s)								
0.03	0.5	0.0	32.8	25.9	185	325	0.00716	0.0059
0.057	0.5	0.0	28.9	21.9	170	305	0.00746	0.0061
0.12	0.5	0.0	24.9	21.4	155	295	0.00752	0.0060
0.057	0.25	0.0	31.5	26.2	150	265	0.01460	0.0121
0.057	0.5	0.0	28.9	21.9	170	305	0.00746	0.0061
0.057	1.0	0.0	25.6	20.9	200	380	0.00339	0.0026
High Diameter (0.5 m) / High Velocity (213.9 m/s)								
0.03	0.5	0.0	107.0	82.0	470	780	0.00706	0.0057
0.057	0.5	0.0	89.0	70.9	415	705	0.00753	0.0062
0.12	0.5	0.0	71.4	59.3	370	645	0.00733	0.0063
0.057	0.25	0.0	97.7	80.1	395	650	0.01274	0.0111
0.057	0.5	0.0	89.0	70.9	415	705	0.00753	0.0062
0.057	1.0	0.0	77.1	59.4	460	790	0.00365	0.0031

TABLE IV.4
SENSITIVITY OF OOMS MODEL PREDICTION TO
VARIATION OF ENTRAINMENT COEFFICIENTS

Gas Jet Density: 4.0 kg/m3 Gas Jet Elevation: 10 m

Entrainment Coefficients α_1 α_2 α_3	Maximum Height, m (3, 6 mps)	Distance to Ground Contact, m (3, 6 mps)	Centerline Concentration at Ground Contact kg/m^3 (3, 6 mps)	
Low Diameter (0.05 m) / Low Velocity (30.6 m/s)				
0.03 0.5 1.0	12.3 11.5	>1000 >1000	0.000001*	0.000002*
0.057 0.5 1.0	12.1 11.4	>1000 >1000	0.000001*	0.000002*
0.12 0.5 1.0	11.7 11.2	>1000 >1000	0.000001*	0.000002*
0.057 0.25 1.0	12.4 11.7	>1000 >1000	0.000001*	0.000002*
0.057 0.5 1.0	12.1 11.4	>1000 >1000	0.000001*	0.000002*
0.057 1.0 1.0	11.7 11.1	>1000 >1000	0.000001*	0.000002*
0.057 0.5 0.5	12.2 11.5	>1000 >1000	0.000002*	0.000008*
0.057 0.5 1.0	12.1 11.4	>1000 >1000	0.000001*	0.000002*
0.057 1.0 2.0	11.9 11.3	>1000 >1000	0.000001*	0.000000*
Typical Diameter (0.2 m) / Typical Velocity (91.7 m/s)				
0.03 0.5 1.0	30.7 24.4	500 >1000	0.000083	0.000060*
0.057 0.5 1.0	27.3 22.5	425 >1000	0.000130	0.000060*
0.12 0.5 1.0	23.7 20.4	370 >1000	0.000180	0.000050*
0.057 0.25 1.0	29.4 24.6	330 >1000	0.000300	0.000060*
0.057 0.5 1.0	27.3 22.5	425 >1000	0.000130	0.000060*
0.057 1.0 1.0	24.5 20.1	615 >1000	0.000030	0.000050*
0.057 0.5 0.5	28.1 23.1	225 550	0.002100	0.000540
0.057 0.5 1.0	27.3 22.5	425 >1000	0.000130	0.000060*
0.057 0.5 2.0	25.9 21.5	>1000 >1000	0.000007*	0.000017*
High Diameter (0.5 m) / High Velocity (213.9 m/s)				
0.03 0.5 1.0	99.5 72.8	645 >1000	0.001220	0.001250*
0.057 0.5 1.0	83.4 63.6	560 >1000	0.001490	0.001100*
0.12 0.5 1.0	71.4 55.6	370 >1000	0.007330	0.000840*
0.057 0.25 1.0	90.7 74.2	510 >1000	0.002530	0.001300*
0.057 0.5 1.0	83.4 63.6	560 >1000	0.001490	0.001100*
0.057 1.0 1.0	73.1 56.3	650 >1000	0.000690	0.000780*
0.057 0.5 0.5	86.1 68.5	470 895	0.003740	0.002000
0.057 0.5 1.0	83.4 63.6	560 >1000	0.001490	0.001100*
0.057 0.5 2.0	78.4 62.2	>1000 >1000	0.000120*	0.000440*

range of release conditions (Table IV.1), with greater sensitivity at lower wind speeds. The predictions of concentration at ground contact are more sensitive to the same variation in α_1 in the presence of atmospheric turbulence entrainment, because the additional entrainment results in the plume remaining aloft to a greater downwind distance. The inclusion of atmospheric turbulence entrainment (assumed Pasquill Stability Class D - Neutral) results in all of the low diameter/low velocity plumes remaining aloft for downwind distances greater than 1000 meters. A similar result is seen for the typical diameter/typical velocity and high diameter/high velocity plume in 6 mps wind. At 3 mps wind, the typical diameter/typical velocity and high diameter/high velocity plumes (centerline) contacts ground at distances less than 1000 m in all except the two cases with the high value for α_3 (2.0). The predictions of maximum rise and distance to ground contact are more sensitive to factor-of-four variation in the coefficient α_2, and the concentration at ground contact changes by factors of about 10 and 4 for the typical diameter/typical velocity, and high diameter/high velocity cases, respectively (when the plume contacts the ground within 1000 meters downwind). Finally, the predictions of maximum rise, distance to ground contact, and concentration at ground contact are sensitive to the prescribed factor-of-four variation in α_3, with the greatest sensitivity to those cases where the plume dilution is dominated by atmospheric turbulence entrainment.

Observations

Ooms' model predictions of maximum rise, distance to ground contact, and concentration at ground contact for a range of elevated dense gas jets considered typical of industrial pressure-relief venting operations, assumed to be released in an atmospheric flow with little or no atmospheric turbulence, are in good agreement with predictions based on the wind tunnel data correlations of Hoot et al.

Ooms' model predictions of the trajectory and dilution of elevated dense gas jets considered typical of industrial pressure-relief venting operations are relatively insensitive to the specification of the jet entrainment coefficient α_1. Model predictions are more sensitive to the

specification of the intermediate field entrainment coefficient α_2; the concentration at ground contact changes by factors of about 4, 6, and 10 for the high diameter/high velocity, typical diameter/typical velocity, and low diameter/ low velocity cases investigated, respectively, when atmospheric turbulence entrainment is discounted ($\alpha_3 = 0$).

Predictions of maximum rise, distance to ground contact, and concentration at ground contact are sensitive to uncertainty in α_3, with the greatest sensitivity to those cases where the plume dilution is dominated by atmospheric turbulence entrainment. For cases where the plume remains aloft, the dilution of the plume is controlled by atmospheric turbulence entrainment after the velocity of the jet decreases to approach the wind velocity. Application of the version of Ooms model presented here to such cases is not recommended, for two reasons:

- the jet/plume cross section is assumed to be circular, rather than elliptical as would be expected (because of lesser entrainment in the vertical than horizontal direction)
- no provision is made for decreased air entrainment which occurs if the bottom of the plume impinges on the ground.

V. DESCRIPTION OF THE DEGADIS DENSE GAS DISPERSION MODEL

The DEGADIS (DEnse GAs DISpersion) model was developed from research sponsored by the U.S. Coast Guard and the Gas Research Institute (Havens and Spicer, 1985). DEGADIS is an adaptation of the Shell HEGADAS model described by Colenbrander (1980) and Colenbrander and Puttock (1983). DEGADIS also incorporates some techniques used by van Ulden (1983).

If the primary source (gas) release rate exceeds the maximum atmospheric takeup rate, a denser-than-air gas blanket is formed over the primary source. This near-field, buoyancy-dominated regime is modeled using a lumped parameter model of a denser-than-air gas "secondary source" cloud which incorporates air entrainment at the gravity-spreading front using a frontal entrainment velocity. If the primary source release rate does not exceed the maximum atmospheric takeup rate, the released gas is taken up directly by the atmosphere and dispersed downwind. For either source condition, the downwind dispersion phase of the calculation assumes a power law concentration distribution in the vertical direction and a modified Gaussian profile in the horizontal direction with a power law specification for the wind profile (Figure V.1). The source model represents a spatially averaged concentration of gas present over the primary source, while the downwind dispersion phase of the calculation models an ensemble average of the concentration downwind of the source.

Denser-than-Air Gas Source Cloud Formation

A lumped parameter model of the formation of the denser-than-air gas source cloud or blanket, which may be formed from a primary source such as an evaporating liquid pool or otherwise specified ground-level emission source, or by an initially specified gas volume of prescribed dimensions for an instantaneous release, is illustrated in Figure V.1. The gas blanket is represented as a cylindrical gas volume which spreads laterally as a density-driven flow with entrainment from the top of the source blanket by wind shear and air entrainment into the advancing

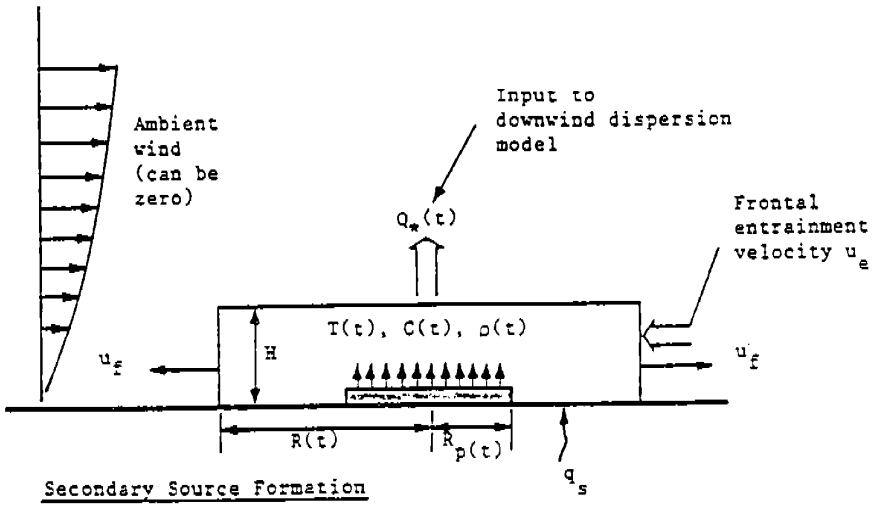

Secondary Source Formation

$$C(x,y,z) = C_C(x)\exp\left[-\left(\frac{|y|-b(x)}{S_y(x)}\right)^2-\left(\frac{z}{S_z(x)}\right)^{1+a}\right], |y| > b$$

$$C(x,y,z) = C_C(x)\exp\left[-\left(\frac{z}{S_z(x)}\right)^{1+a}\right], |y| \le b$$

$$u_x = u_0\left(\frac{z}{z_0}\right)^a$$

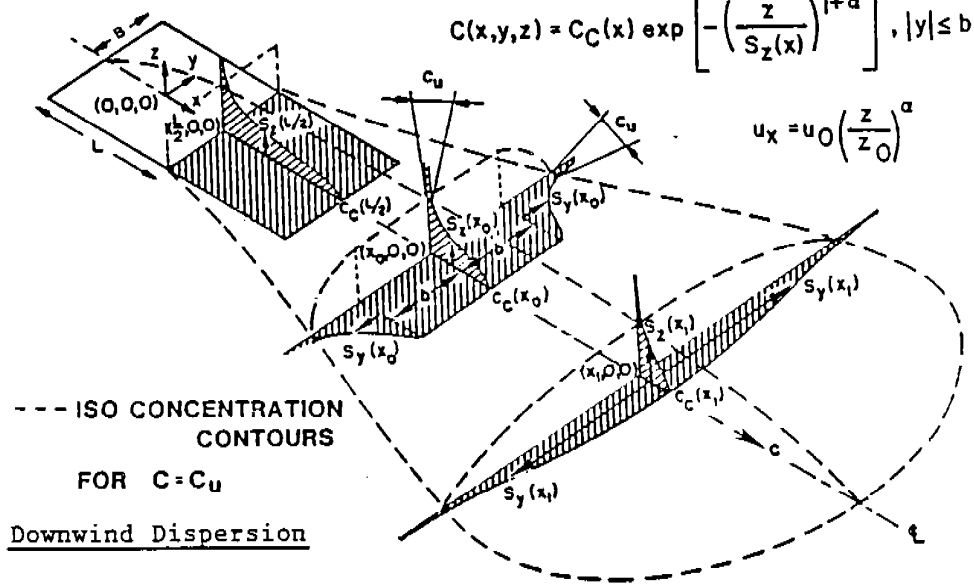

--- ISO CONCENTRATION CONTOURS

FOR $C = C_u$

Downwind Dispersion

Figure V.1. Schematic diagram of DEGADIS dense gas dispersion model.

front edge. The source blanket will continue to grow over the primary source until the atmospheric takeup rate from the top is matched by the air entrainment rate from the side and, if applicable, by the rate of gas addition from under the blanket. Of course, the blanket is not formed if the atmospheric takeup rate is greater than the evolution rate of the primary source. For application of the downwind calculation procedure, the blanket is modeled as being stationary over the center of the source ($x = 0$).

Secondary Source Blanket Extent for Ground Level Releases

If a denser-than-air gas blanket is present, the (downwind) emission rate from the blanket is equal to the maximum atmospheric takeup rate. That is, for $E(t)/\pi R_p^2(t) > Q_{*max}$, a source blanket is formed over the primary source. The blanket frontal (spreading) velocity is modeled as

$$u_f = C_E \sqrt{g \left[\frac{\rho - \rho_a}{\rho_a}\right] H} \qquad (V.1)$$

where ρ is the average density of the source blanket. This gravity intrusion relationship is applicable only for $\rho > \rho_a$; the value of C_E used is 1.15 based on laboratory measurements of cloud spreading velocity (Havens and Spicer, 1985).

The blanket radius R as a function of time is determined by integrating $dR/dt = u_f$. When the total mass of the cloud is decreasing with time, the radius is assumed to decrease according to $(dR/dt)/R = (dH/dt)/H$ for ground-level sources. The radius of the blanket is constrained to be greater than or equal to the radius R_p of any primary (liquid) source present.

Secondary Source Blanket Extent for Instantaneous Releases

The gravity intrusion relationship (Equation (V.1)) will overpredict initial velocities for instantaneous, aboveground releases of a denser-than-air gas since no initial acceleration phase is included. In this

case, the following procedure adapted from van Ulden (1983) is recommended.

For instantaneous gas releases, the radially symmetric cloud is considered to be composed of a tail section with height H_t and radius R_h and a head section with height H_h (Figure V.2). A momentum balance is used to account for the acceleration of the cloud from rest; the effect of ambient (wind) momentum is ignored. Although the following equations are derived assuming the primary source emission rate is zero, the resulting equations are assumed to model the secondary source cloud development when the primary source rate is nonzero. When the frontal velocity from the momentum balance is the same as Equation (V.1), the momentum balance is no longer applied and the frontal velocity is given by Equation (V.1).

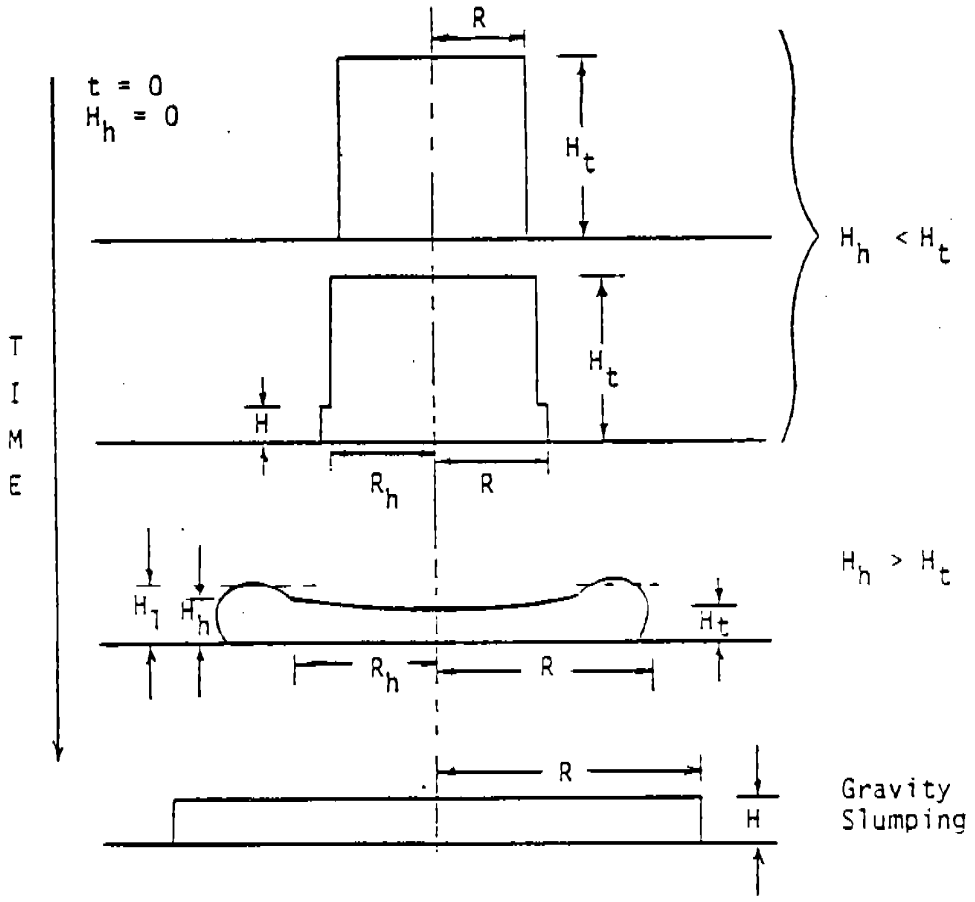

Figure V.2. Schematic diagram of a radially spreading cloud.

There are three main forces acting on the cloud: a static pressure force (F_p), a dynamic drag force (F_d), and a force which accounts for the acceleration reaction of the ambient fluid, represented as a rate of virtual momentum change with respect to time ($-dP_v/dt$). Denoting the momentum of the head and tail as P_h and P_t, respectively, the momentum balance is

$$\frac{dP}{dt} = \frac{d}{dt}(P_h + P_t) = F_p + F_d - \frac{dP_v}{dt} \qquad (V.2)$$

or

$$\frac{d}{dt}(P_h + P_t + P_v) = F_p + F_d \qquad (V.3)$$

The terms in the momentum balance are evaluated differently for early times before a gravity current head has developed ($H_h < H_t$) and for times after the head has developed but the cloud is still accelerating (Figure V.2). Because the gravity current head develops so rapidly, the model equations describing the times after the gravity current head forms ($H_h \geq H_t$) are derived first. The model equations describing earlier times ($H_h < H_t$) use simplification of the equations for $H_h \geq H_t$.

Unsteady Gravity Current

When the cloud accelerates to the point that $H_h \geq H_t$ (Figures V.2, V.3), the frontal velocity is determined from the momentum balance (Equation (V.2)) as follows.

Figure V.3. The unsteady gravity current (van Ulden, 1983).

The static pressure force, obtained by integrating the static pressure over the boundary of the current, is

$$F_p = \left(\frac{1}{2} g\Delta\rho H_t \right) \left(2\pi R H_t \right) = \pi g \Delta\rho R H_t^2 \qquad (V.4)$$

Neglecting the shear stress at the bottom, the dynamic force on the current is the sum of the drag force on the head of the current and the lift force that arises due to asymmetry in the ambient flow around the head. The drag force is represented by

$$F_D = - \frac{d_v}{2} \rho_a u_f^2 \left(2\pi R_h a_v H_h \right) = -a_v d_v \pi R H_h \rho_a u_f^2 \qquad (V.5)$$

where d_v is an effective drag coefficient and the constant a_v is an empirical ratio of the average head depth H_1 to H_h ($a_v = H_1/H_h$).

The horizontal acceleration reaction ($-dP_v/dt$) is approximated by the reaction to an accelerating elliptical cylinder with an aspect ratio H/R (Batchelor, 1967):

$$-\left(\frac{dP_v}{dt}\right)_R = -\frac{d}{dt}\left(k_1\rho_a\pi RH^2u_f\right) \tag{V.6}$$

and the vertical acceleration reaction is represented as

$$-\left(\frac{dP_v}{dt}\right)_z = -\frac{d}{dt}\left(k_2\rho_a\pi RH^2u_f\right) \tag{V.7}$$

where k_1 and k_2 are coefficients of order one. Using a single constant, Equations (V.6) and (V.7) give

$$-\frac{dP_v}{dt} = -e_v\pi\rho_a\frac{d(RH^2u_f)}{dt} \tag{V.8}$$

Using Equations (V.4), (V.5), and (V.8), the momentum balance (Equation (V.2)) becomes

$$\frac{dP}{dt} = \pi g\Delta\rho RH_t^2 - a_v d_v \pi\rho_a RH_h u_f^2 - e_v\pi\rho_a\frac{d(RH^2u_f)}{dt} \tag{V.9}$$

Following van Ulden (1979, 1983), it is assumed that the potential energy decrease due to slumping of the cloud is offset by the production of kinetic energy, which through the action of shear, is partly transformed to turbulent kinetic energy. Part of the turbulent kinetic energy is transformed back into potential energy due to entrainment of air by the cloud. This "buoyant destruction" of kinetic energy is assumed to be proportional to the rate of production of turbulent kinetic energy, and following Simpson and Britter (1979) it is assumed that the turbulent kinetic energy production rate scales as $\pi\rho_a HRu_f^3$. Then,

$$\frac{1}{2}g\Delta\rho H\frac{dV}{dt} = \epsilon\pi\rho_a HRu_f^3 \tag{V.10}$$

which can be written

$$\frac{dV}{dt} = \frac{\epsilon(2\pi RH)u_f}{\left[\frac{g\Delta\rho H}{\rho_a u_f^2}\right]} = \frac{\epsilon(2\pi RH)u_f}{Ri_f} \tag{V.11}$$

where ϵ is an empirically determined coefficient. Noting dV/dt represents the air entrainment rate,

$$\frac{\dot{M}_a}{\rho_a} = \epsilon(2\pi RH)u_f \Big/ \left[\frac{g\Delta\rho H}{\rho_a u_f^2} \right] \tag{V.12}$$

where $\dot{M}_a$ represents the air entrainment mass rate.

The volume integral

$$V = 2\pi \int_0^R h(r,t)rdr \tag{V.13}$$

where h(r,t) is to be expressed in terms of H_h and H_t, and the momentum integral

$$P = 2\pi \int_0^R \rho u(r,t)h(r,t)rdr = P_t + P_h \tag{V.14}$$

are then approximated with separate analyses of the head and tail of the current.

In the tail of the current, the shallow water equations are assumed applicable. It is assumed that the shape of the current is quasi-stationary in time, and the layer-averaged density difference is assumed horizontally uniform. It follows that the volume and momentum of the tail are given by

$$V_t = \pi R_h^2 \left[H_t + H_h \right] / 2. \tag{V.15}$$

$$P_t = \frac{2}{5} \rho \left[\frac{2}{3} H_t + H_h \right] \pi R_h^3 \frac{u_f}{R} \tag{V.16}$$

A momentum balance for the head region, Figure V.4, assuming quasi-steady state, indicates that the static and dynamic pressure forces on the head should be balanced by the net flux of momentum due to flow into and out of the head. The static pressure and drag are, respectively

$$F_p = \left[\frac{1}{2} g\Delta\rho H_h \right] \left[2\pi R_h H_h \right] = \pi g\Delta\rho R_h H_h^2 \tag{V.17}$$

$$F_D = - d_v \left(\frac{1}{2} \rho_a u_f^2 \right) \left[2\pi R_h (a_v H_h) \right]$$

$$= - a_v d_v \rho_a u_f^2 \pi R_h H_h \qquad (V.18)$$

Near the surface, the inward flow (u_4 in Figure V.4) carries momentum into the head, while the return flow (u_3 in Figure V.4) carries momentum out of the head. Assuming $u_3 \simeq u_4$, $H_4 \simeq 1/2\ H_h$, and $u_4 \simeq \delta_v u_f$, the momentum flux into the head is approximately

$$Q_h \simeq \delta_v^2 \rho_a u_f^2 \left[2\pi R_h H_h \right] \qquad (V.19)$$

Figure V.4. The head of a steady gravity current (Simpson and Britter, 1979; van Ulden, 1983).

Upon rearranging, the momentum balance on the head gives

$$\frac{\rho_a u_f^2}{g \Delta\rho H_h} = 1./\left(a_v d_v - 2\delta_v^2 \right) = C_E^2 \qquad (V.20)$$

when $\delta_v = 0.2$ and $d_v = 0.64$; Equation (V.20) then specifies the head velocity boundary condition. The volume of the head is determined by assuming that the head length scales with H_1. It follows that

$$R - R_h = b_v H_1 \tag{V.21}$$

where b_v is an empirical constant, and the volume of the head becomes

$$V_h = \pi a_v b_v (R + R_h) H_h^2 \tag{V.22}$$

If the layer-averaged velocity is assumed to increase linearly with r, it follows that

$$u_h = u_f \left(\frac{R_h}{R} \right) \tag{V.23}$$

and

$$P_h = \frac{2\pi}{3} \rho a_v \frac{u_f H_h}{R} \left[R^3 - R_h^3 \right] \tag{V.24}$$

Along with the definition of u_f,

$$\frac{dR}{dt} = u_f, \tag{V.25}$$

Equations (V.9), (V.11), (V.20), (V.21), (V.23), and (V.25) are solved to determine ρ, H_t, H_h, V, P_h, and P_t when $H_h > H_t$.

The constants a_v, b_v, d_v, e_v, and ϵ are assigned values 1.3, 1.2, 0.64, 20., and 0.59, respectively, based on analysis of the still-air denser-than-air gas release experiments of Havens and Spicer (1985).

Initial Gravity Current Development

In order to model the initial cloud shape, the tail and head height are considered constant with respect to radius. The momentum balance on the cloud is then given by

$$\frac{d}{dt}\left[P_h + P_t \right] = \pi g \Delta\rho \left[R_h H_t^2 + a_v b_v H_h^3 \right]$$

$$- \pi a_v d_v \rho_a R H_h u_f^2 - \frac{dP_v}{dt} \qquad (V.26)$$

where the first term on the right-hand side represents the static pressure force on the head and the second term represents the drag force on the bottom surface of the cloud. The third force is the acceleration reaction by the ambient fluid, represented by Equation (V.8).

The dimensions of the head are again given by

$$R_h = R - a_v b_v H_h \qquad (V.27)$$

and

$$H_h = \left(\frac{u_f}{C_E} \right)^2 \Big/ \left[g\Delta\rho/\rho_a \right] \qquad (V.28)$$

When the height of the tail H_t is assumed uniform with respect to radius, it follows that

$$H_t = \left[\frac{M}{\rho} - \pi a_v^2 b_v \left(R + R_h \right) H_h^2 \right] \Big/ \left(\pi R_h^2 \right) \qquad (V.29)$$

where M is the total mass of the cloud. The momentum of the head P_h and tail P_t are then

$$P_h = \frac{2}{3} \pi a_v \frac{\rho H_h \left(R^3 - R_h^3 \right)}{R} u_f \qquad (V.30)$$

and

$$P_t = \frac{2}{3} \pi \frac{\rho H_t R_h^3}{R} u_f \qquad (V.31)$$

Equations (V.26) through (V.31) determine the momentum of the blanket as a function of time, and thus the frontal velocity u_f. The cloud accelerates from rest because $H_h = 0$ initially.

Material and Energy Balances

The balance on the total mass of gas in the source blanket ($M = \pi R2H\rho$) is

$$\frac{dM}{dt} = \frac{d}{dt}\left[\pi R^2 H\rho\right] = \frac{E(t)}{w_{c,p}(t)} + \dot{M}_a + \dot{M}_{w,s} - \left[\frac{Q_{*max}}{w_c}\right]\left(\pi R^2\right) \tag{V.32}$$

where $E(t)$ is the contaminant evolution rate from the primary (liquid) source and $w_{c,p}(t)$ is the contaminant mass fraction in the primary source. For spills over water, the water entrainment term ($M_{w,s}$) is included in the source blanket description and is calculated from Equation (V.46), and the (humid) air entrainment rate (Equation (V.12)) is

$$\dot{M}_a = 2\pi RH(\epsilon u_f)\rho_a \Big/ \left[g\Delta\rho H/(\rho_a u_f^2)\right] \tag{V.33}$$

The balance on the mass of contaminant in the source blanket ($M_c = w_c \pi R^2 H\rho$) is

$$\frac{dM_c}{dt} = \frac{d}{dt}\left[w_c \pi R^2 H\rho\right] = E(t) - Q_{*max}\left(\pi R^2\right) \tag{V.34}$$

and the mass balance on the air in the source blanket ($M_a = w_a \pi R^2 H\rho$) is

$$\frac{dM_a}{dt} = \frac{d}{dt}\left[w_a \pi R^2 H\rho\right] = \frac{E(t)}{w_{c,p}(t)}\left[\frac{1 - w_{c,p}(t)}{1 + H_a}\right] + \frac{\dot{M}_a}{1 + H_a} - \left[\frac{Q_{*max}}{w_c}\right] w_a \left(\pi R^2\right) \tag{V.35}$$

where the ambient humidity is H_a and the mass fraction of contaminant and air are $w_c = M_c/M$ and $w_a = M_a/M$, respectively. Note that any dilution with air of the primary source is assumed to be with the ambient humidity.

The energy balance on the source blanket ($h\pi R^2 H\rho$) gives

$$\frac{d}{dt}\left[h\pi R^2 H\rho \right] = \frac{h_p\, E(t)}{w_{c,p}(t)} + h_a \dot{M}_a + h_w \dot{M}_{w,s} - h\left[\frac{Q_{*max}}{w_c}\right](\pi R^2) + \dot{Q}_s \qquad (V.36)$$

where h_p is the enthalpy of the primary source gas, h_a is the enthalpy of the ambient humid air, and h_w is the enthalpy of any water vapor entrained by the blanket if over water. There are three alternate submodels included for the heat transfer ($\dot{Q}_s$) from the surface to the cloud.

The simplest method for calculating the heat transfer between the substrate and the gas cloud is to specify a constant heat transfer coefficient for the heat transfer relation

$$\dot{Q}_s = q_s\left[\pi\left(R^2 - R_p^2\right)\right] = h_0 \Delta T\left[\pi\left(R^2 - R_p^2\right)\right] \qquad (V.37)$$

where $\dot{Q}_s$ is the rate of heat transfer to the cloud, q_s is the heat flux, and ΔT is the temperature difference between the cloud and the surface. For the calculation of heat transfer over the source, the temperature difference is based on the average temperature of the blanket.

In the evaluation of the Burro and Coyote series of experiments, Koopman et al. (1981) proposed the following empirical heat transfer coefficient relationship for heat transfer between a cold LNG cloud and the ground

$$h_0 = V_H \rho C_p \qquad (V.38)$$

where the value of V_H was estimated to be 0.0125 m/s. This constant can be varied in the model.

From the heat transfer coefficient descriptions for heat transfer from a flat plate, the following relationships can be applied. For natural convection, the heat transfer coefficient is estimated using the Nusselt (Nu), Grashoff (Gr), and Schmidt (Sc) numbers (McAdams, 1954) from

$$Nu = 0.14\,(Gr\ Sc)^{1/3} \qquad (V.39)$$

Or

$$h_n = 0.14 \left[\frac{g\rho^2 C_p^3 \mu}{T\ Pr^2} \Delta T \right]^{1/3} \qquad (V.40)$$

where h_n is the heat transfer coefficient due to natural convection and Pr is the Prandtl number. In order to simplify the calculations, the parameter group

$$\left[Pr^{-2} \left(C_p MW \right)^3 \left(\frac{\mu}{MW\ T} \right) \right]^{1/3} \qquad (V.41)$$

is estimated to be 60 in mks units. The actual value of the group is 47.25, 58.5, and 73.4 for air, methane, and propane, respectively. Equation (V.40) becomes

$$h_n = 18 \left[\left(\frac{\rho}{MW} \right)^2 \Delta T \right]^{1/3} \qquad (V.42)$$

where the density ρ, molecular weight MW, and temperature difference ΔT are based on the average composition of the gas blanket.

For forced convection, the Colburn analogy (Treybal, 1980) is applied to a flat plate using the Stanton number for heat transfer St_H and the Prandtl number as

$$St_H\ Pr^{2/3} = \frac{c_f}{2} = \left(\frac{u_*}{\bar{u}} \right)^2 \qquad (V.43)$$

Or

$$h_f = (\bar{u}\rho C_p)\ Pr^{-2/3} \left(\frac{u_*}{\bar{u}} \right)^2 \qquad (V.44)$$

where h_f is the heat transfer coefficient due to forced convection. If the velocity is evaluated at z = H/2 and Pr is estimated to be 0.741,

$$h_f = \left[1.22 \frac{u_*^2}{u_0} \left(\frac{2z_0}{H} \right)^{\alpha} \right] \rho C_p \qquad (V.45)$$

If $H/2 < z_R$, then the velocity is evaluated at $z = z_R$.

The overall heat transfer coefficient is then the maximum of the forced and natural coefficients, i.e. $h_0 = \max(h_f, h_n)$. The heat flux and transfer rate are then estimated by Equation (V.37).

If the gas blanket is formed over water, water will be transferred from the surface to the cloud by a partial pressure driving force associated with the temperature difference between the surface and the gas blanket. The rate of mass transfer of water is

$$\dot{M}_{w,s} = \frac{F_0}{p} \left(p^*_{w,s} - p_{w,c} \right) \left[\pi \left(R^2 - R_p^2 \right) \right] \qquad (V.46)$$

where F_0 is the overall mass transfer coefficient. The driving force is the difference of the ~~vapor~~ pressure of water at the surface temperature $p^*_{w,s}$ and the partial pressure of water in the cloud, $p_{w,c}$. (The water partial pressure in the cloud is the minimum of: (a) the water mole fraction times the ambient pressure; or (b) the water vapor pressure at the cloud temperature ($p^*_{w,c}$).) The natural convection coefficient is based on the heat transfer coefficient and the analogy between the Sherwood number (Sh) and the Nusselt number (Nu) suggested by Bird et al. (1960)

$$Sh = Nu = 0.14 \, (Gr \, Sc)^{1/3} = \frac{F_n L}{\mathcal{D}} \left(\frac{MW}{\rho} \right) \qquad (V.47)$$

If the Schmidt number is taken as 0.6, and $\left(\frac{\mu}{T \, MW} \right)$ is estimated to be 2.2×10^{-9} in mks units,

$$F_n = 9.9 \times 10^{-3} \left[\left(\frac{\rho}{MW} \right)^2 \Delta T \right]^{1/3} \qquad (V.48)$$

For forced convection, Treybal (1980) suggests that the Stanton number for mass transfer St_M and the Stanton number for heat transfer St_H are related by

$$St_M = St_H \left(\frac{Pr}{Sc} \right)^{2/3} = 1.15 \, St_H \qquad (V.49)$$

Or,

$$F_f = \frac{20.7\ h_0}{MW\ C_p} \qquad (V.50)$$

The overall mass transfer coefficient F_0 is calculated as the larger of the natural and forced convection coefficients.

For the case when the primary (liquid) source emission rate E(t) is larger than the atmospheric takeup rate $Q_{*max}\pi R_p^2$, Equations (V.32), (V.34), (V.35), and (V.36) are integrated for the mass, concentration, and enthalpy of the gas blanket along with an appropriate equation of state (i.e. relationship between enthalpy and temperature and between temperature and density).

For the case when the emission rate is not sufficient to form a gas blanket, the flux of contaminant is not determined by the maximum atmospheric takeup rate. Consider the boundary layer formed by the emission of gas into the atmosphere above the primary source. If the source is modeled to have a uniform width 2b and entrain no air along the sides of the layer, the balance on the total material ($\rho_L u_L H_L$) in a differential slice of the layer is

$$\frac{d}{dx}\left[\ \rho_L u_L H_L\ \right] = \rho_a w_e + \left(\frac{Q_*}{w_c}\right)_p \qquad (V.51)$$

where w_e is the vertical rate of of air entrainment into the layer given by Equation (V.83), ρ_L is the average density of the slice, and $(Q_*/w_c)_p$ is the total flux of gas from the primary (liquid) source. The balance on the mass flow rate of contaminant ($w_c \rho_L u_L H_L$) at any ($x - x_{up}$) is

$$c_{c,L} u_L H_L = Q_*(x - x_{up}) \qquad (V.52)$$

With an equation of state to relate $c_{c,L}$ and ρ_L, Equation (V.51) is integrated from the upwind edge of the source ($x = x_{up}$) to the downwind edge ($x = L + x_{up}$).

In order to generate the initial conditions for the downwind dispersion calculations, the maximum concentration c_c and the vertical dispersion parameter S_z are needed. Since Equations (V.51) and (V.52) are written for a vertically averaged layer, consider the vertical

average of the power law distribution. The height of the layer H_L is the height to some concentration level, say 10% of the maximum. Although strictly a function of α, this value is modeled by

$$H_L = \delta_L H_{EFF} \tag{V.53}$$

where H_{EFF} is the effective height defined by Equation (V.79) and δ_L is 2.15. The vertically averaged concentration $c_{c,L}$ can be defined by

$$c_{c,L} H_L = \int_0^\infty c\,dz \tag{V.54}$$

And similarly, the effective transport velocity u_L is defined by

$$c_{c,L} u_L H_L = \int_0^\infty c u_x\,dz \tag{V.55}$$

With Equation (V.53) and defining relations for H_{EFF} and u_{EFF} (Equations (V.79) and (V.93), respectively), it follows that

$$c_c = \delta_L c_{c,L} \tag{V.56}$$

$$u_L H_L = \delta_L \left(\frac{u_0 z_0}{1+\alpha} \right) \left(\frac{S_z}{z_0} \right)^{1+\alpha} \tag{V.57}$$

and

$$\delta_L w_e' = w_e \tag{V.58}$$

where w_e' is given by Equation (V.83).

Maximum Atmospheric Takeup Rate

The maximum atmospheric takeup rate will be the largest takeup rate which satisfies Equations (V.51) and (V.52). As well, the maximum concentration of contaminant in the power law profile at the downwind edge of the source will be the source contaminant concentration $(c_c)_s$. If Equations (V.51) and (V.52) are combined along with the assumption of adiabatic mixing of ideal gases with the same constant molal heat

capacity (i.e. $\left[\frac{\rho - \rho_a}{c_c}\right] = \gamma$ = constant), the maximum takeup flux is modeled by

$$Q_{*max} = (c_c)_s \frac{ku_*(1 + \alpha)}{\hat{\phi}} \left[\frac{\delta_L}{\delta_L - 1}\right] \tag{V.59}$$

where

$$\frac{1}{\hat{\phi}} = \frac{1}{L}\int_0^L \frac{dx}{\phi(Ri_*)} \tag{V.60}$$

where $\phi(Ri_*)$ is given in Equation (V.76) for $\rho > \rho_a$.

An upper bound of the atmospheric takeup flux can be characterized by the condition where the source begins to spread as a gravity intrusion against the approach flow. In water flume experiments, Britter (1980) measured the upstream and lateral extent of a steady-state plume from a circular source as a function of Ri_*. A significant upstream spread was obtained for $Ri_* > 32$, and lateral spreading at the center of the source was insignificant for $Ri_* < 8$. The presence of any significant lateral spreading represents a lower bound on the conditions of the maximum takeup flux.

The integral of Equation (V.60) is calculated using a local Richardson number of

$$Ri_*(x) = \zeta(x - x_{up})^{\frac{1}{1+\alpha}} \tag{V.61}$$

where

$$\zeta = g\left[\frac{\rho - \rho_a}{\rho_a}\right]\frac{z_0}{u_*^2}\frac{\Gamma\left[\frac{1}{1+\alpha}\right]}{1+\alpha}\left[\frac{ku_*(1 + \alpha)}{\phi_c}\left[\frac{1 + \alpha}{u_0 z_0}\right]\left[\frac{\delta_L}{\delta_L - 1}\right]\right]^{\frac{1}{1+\alpha}} \tag{V.62}$$

and ϕ_c is 3.1 (corresponding to $Ri_* = 20 (8 < Ri_* < 32)$). Using this $Ri_*(x)$, Equation (V.60) is

$$\frac{1}{\hat{\phi}} = \frac{1}{L}\int_0^L \frac{dx}{0.88 + 0.099\ \zeta^{1.04}\ x^{\frac{1.04}{1+\alpha}}}$$

In order to simplify the numerical problem, the integral is approximated as

$$\frac{1}{\hat{\phi}} = \frac{1}{0.099\ L\ \zeta^{1.04}} \ln\left[\frac{0.88 + 0.099\ \zeta^{1.04}\ L^{\left(\frac{1.04}{1+\alpha}\right)}}{0.88}\right] \qquad (V.63)$$

which then specifies the maximum atmospheric takeup flux.

Transient Denser-than-Air Gas Release Simulation

If a steady-state spill is being simulated, the transient source calculation is carried out until the source characteristics are no longer varying significantly with time. The maximum centerline concentration c_c, the horizontal and vertical dispersion parameters S_y and S_z, the half width b, and if necessary, the enthalpy h are used as initial conditions for the downwind calculation specified in a transient spill.

If a transient spill is being simulated, the spill is modeled as a series of pseudo-steady-state releases. Consider a series of observers traveling with the wind over the transient gas source described above; each observer originates from the point which corresponds with the maximum upwind extent of the gas blanket ($x = -R_{max}$). The desired observer velocity is the average transport velocity of the gas u_{EFF} from Equation (V.93); however, the value of u_{EFF} will differ from observer to observer with the consequence that some observers may be overtaken by others. For a neutrally buoyant cloud, u_{EFF} becomes a function of downwind distance alone which circumvents this problem. With this functionality, Colenbrander (1980) models the observer velocity as

$$u_i(x) = \frac{u_0}{\Gamma\left(\frac{1}{1+\alpha}\right)} \left(\frac{S_{z_{0m}}}{z_0} \right)^{\alpha} \left[\frac{x + R_{max}}{\frac{\sqrt{\pi}}{2} R_m + R_{max}} \right]^{\alpha/(1+\alpha)} \tag{V.64}$$

where $S_{z_{0m}}$ is the value of S_{z_0} when the averaged source rate ($\pi R^2 Q_*$) is a maximum and the subscript i denotes observer i. Noting that $u_i(x) = dx_i/dt$, observer position and velocity as functions of time are determined.

A pseudo-steady-state approximation of the transient source is obtained as each observer passes over the source. If t_{up_i} and t_{dn_i} denote the times when observer i encounters the upwind and downwind edges of the source respectively, then the source fetch seen by observer i is:

$$L_i = x_{up_i} - x_{dn_i} \tag{V.65}$$

The width of the source $2B_i'(t)$ is defined by

$$B_i'^2(t) = R^2(t) - x_i^2(t) \tag{V.66}$$

Then the gas source area seen by observer i is

$$2L_i b_i = 2 \int_{t_{up_i}}^{t_{dn_i}} B_i' u_i dt \tag{V.67}$$

where $2b_i$ is the average width.

The takeup rate of contaminant $2(Q_* Lb)_i$ is calculated as

$$2(Q_* Lb)_i = 2 \int_{t_{up_i}}^{t_{dn_i}} Q_* B_i' u_i dt \tag{V.68}$$

The total mass flux rate from the source is

$$2(\rho_L u_L H_L b)_i = 2 \int_{t_{up_i}}^{t_{dn_i}} \left(\rho_a w_e' + \left(\frac{Q_*}{w_c} \right) \right) B_i' u_i dt \tag{V.69}$$

With these equations, the average composition of the layer can be determined at each $x - x_{up}$ over the source. With the enthalpy of the layer given by

$$2(h_L \rho_L u_L H_L b)_i = 2 \int_{t_{up_i}}^{t_{dn_i}} h \left(\frac{Q_*}{w_c} \right) B_i' u_i dt \qquad (V.70)$$

(due to the choice of the reference temperature as the ambient temperature) and with a suitable equation of state relating enthalpy, temperature, and density, the source can be averaged for each observer. After the average composition of the layer is determined at the downwind edge, an adiabatic mixing calculation is performed between this gas and the ambient air. This calculation represents the function between density and concentration for the remainder of the calculation if the calculation is adiabatic; it represents the adiabatic mixing condition if heat transfer is included in the downwind calculation.

For each of several observers released successively from $x = -R_{max}$, the observed dimensions L and b, the downwind edge of the source x_{dn}, the average vertical dispersion coefficient S_z, the average takeup flux Q_*, the centerline concentration c_c, and if applicable, the average enthalpy h_L can be determined for each observer. With these input values, a steady-state calculation is made for each observer. The distribution parameters for any specified time t_s are determined by locating the position of the series of observers at time t_s, i.e. $x_i(t_s)$. The corresponding concentration distribution is then computed from the assumed profiles.

Steady-State Downwind Dispersion

The model treats dispersion of gas entrained into the wind field from an idealized, rectangularly shaped source of width 2b and length L. The circular source cloud is represented as an equivalent area rectangle ($\pi R^2 = 2bL$) with equivalent fetch ($L = 2R$). Similarity forms for the concentration profiles are assumed which represent the plume as being composed of a horizontally homogeneous section with Gaussian concentration profile edges as follows:

$$c(x,y,z) = c_c(x) \exp\left[- \left(\frac{|y| - b(x)}{S_y(x)} \right)^2 - \left(\frac{z}{S_z(x)} \right)^{1+\alpha} \right] \qquad \text{for } |y| > b$$

$$= c_c(x) \exp\left[- \left(\frac{z}{S_z(x)} \right)^{1+\alpha} \right] \qquad \text{for } |y| \leq b \tag{V.71}$$

A power law wind velocity profile is assumed

$$u_x = u_0 \left(\frac{z}{z_0} \right)^{\alpha} \tag{V.72}$$

where the value of α is determined by a weighted least-squares fit of the logarithmic profile

$$u_x = \frac{u_*}{k} \left[\ln \left(\frac{z + z_R}{z_R} \right) - \psi \left(\frac{z}{\lambda} \right) \right] \tag{V.73}$$

Functional forms for ψ and typical values of α are given in Table V.1 for different Pasquill stability categories. With these profiles, the parameters of Equation (V.71) are constrained by ordinary differential equations.

Vertical Dispersion

The vertical dispersion parameter S_z is determined by requiring that it satisfy the diffusion equation

TABLE V.1. TYPICAL ATMOSPHERIC BOUNDARY LAYER STABILITY AND WIND PROFILE CONCENTRATIONS

Pasquill Stability Category	Monin-Obukhov Length (λ) as a Function of Surface Roughness z_R(m)[1]	Typical Power Law Exponents α in Eq. (B-72)	Corrections to Logarithmic Profiles as Given by Businger et al. (Reference 20) ψ in Eq. (B-73)
A	$-11.4\ z_R^{0.10}$	0.108	$\psi = 2\ln\left[\frac{1+a}{2}\right] + \ln\left[\frac{1+a^2}{2}\right] - 2\tan^{-1}(a) + \frac{\pi}{a}$, with $a = (1-15(z/\lambda))^{1/4}$
B	$-26.0\ z_R^{0.17}$	0.112	
C	$-123\ z_R^{0.30}$	0.120	
D	∞	0.142	$\psi = 0$
E	$123\ z_R^{0.30}$	0.203	$\psi = -4.7(z/\lambda)$
F	$26.0\ z_R^{0.17}$	0.253	

[1] Curve fit of data from Pasquill (Reference 17).

$$u_x \frac{\partial c}{\partial x} = \frac{\partial}{\partial z} K_z \frac{\partial c}{\partial z} \tag{V.74}$$

with the vertical turbulent diffusivity given by

$$K_z = \frac{k u_* z}{\phi(Ri_*)} \tag{V.75}$$

The function $\phi(Ri_*)$ is a curve fit of laboratory-scale data for vertical mixing in stably density-stratified fluid flows reported by Kantha et al. (1977), Lofquist (1960), and McQuaid (1976) for $Ri_* > 0$. For $Ri_* < 0$, the function $\phi(Ri_*)$ is taken from Colenbrander and Puttock (1983) and has been modified so the passive limit of the two functions agree as follows:

$$\begin{aligned} \phi(Ri_*) &= 0.88 + 0.099\ Ri_*^{1.04} && Ri_* \geq 0 \\ &= 0.88/(1 + 0.65\ |Ri_*|^{0.6}) && Ri_* < 0 \end{aligned} \tag{V.76}$$

The friction velocity is calculated using Equation (V.73) from a known velocity u_0 at a specific height z_0. Combining the assumed similarity forms for concentration and velocity, Equations (V.71), (V.72), (V.74), and (V.75) give

$$\frac{d}{dx}\left[\left(\frac{u_0 z_0}{1+\alpha}\right)\left(\frac{S_z}{z_0}\right)^{1+\alpha}\right] = \frac{k u_* (1+\alpha)}{\phi(Ri_*)} \tag{V.77}$$

where the Richardson number Ri_* is computed as

$$Ri_* = g\left(\frac{\rho - \rho_a}{\rho_a}\right)\frac{H_{EFF}}{u_*^2} \tag{V.78}$$

and the effective cloud depth is defined as

$$H_{EFF} = \frac{1}{c_c}\int_0^\infty c\,dz = \Gamma\left(\frac{1}{1+\alpha}\right)\frac{S_z}{1+\alpha} \tag{V.79}$$

Equation (V.77) can be viewed as a volumetric balance on a differential slice of material downwind of the source. For a mass balance over the same slice,

$$\frac{d}{dx}\left[\rho_L u_L H_L\right] = \rho_a w_e \tag{V.80}$$

which is the same result as Equation (V.51) without the source term. With Equations (V.57) and (V.58), this becomes

$$\frac{d}{dx}\left[\rho_L u_{EFF} H_{EFF}\right] = \rho_a w_e' \tag{V.81}$$

Using the assumption of adiabatic mixing of ideal gases with the same constant molal heat capacity (i.e. $\frac{\rho - \rho_a}{c_c}$ = constant) along with the contaminant material balance, the mass balance becomes

$$\frac{d}{dx}\left[u_{EFF} H_{EFF}\right] = w_e' \tag{V.82}$$

which leads to

$$w_e' = \frac{w_e}{\delta_L} = \frac{k u_* (1 + \alpha)}{\phi(Ri_*)} \tag{V.83}$$

Equations (V.81) and (V.83) are combined to give

$$\frac{d}{dx}\left[\rho_L u_{EFF} H_{EFF}\right] = \frac{\rho_a k u_* (1 + \alpha)}{\phi(Ri_*)} \tag{V.84}$$

Furthermore, Equation (V.84) is assumed to apply when $(\rho - \rho_a)/c_c$ is not constant.

When heat transfer from the surface is present, vertical mixing will be enhanced by the convection turbulence due to heat transfer. Zeman and Tennekes (1977) model the resulting vertical turbulent velocity as

$$\frac{w}{u_*} = \left[1 + \frac{1}{4}\left(\frac{w_*}{u_*}\right)^2\right]^{1/2} \tag{V.85}$$

where w_* is the convective scale velocity described as

$$\left(\frac{w_*}{u_*} \right)^2 = \left[\frac{gh}{u_* \bar{u}} \frac{\left(T_s - T_{c,L} \right)}{T_{c,L}} \right]^{2/3} \tag{V.86}$$

If $\bar{u}$ is is evaluated at H_{EFF},

$$\frac{w}{u_*} = \left(1 + \frac{1}{4} Ri_T^{2/3} \right)^{1/2} \tag{V.87}$$

where

$$Ri_T = g \left(\frac{T_s - T_{c,L}}{T_{c,L}} \right) \frac{H_{EFF}}{u_* u_0} \left(\frac{z_0}{H_{EFF}} \right)^{\alpha} \tag{V.88}$$

and $T_{c,L}$ is the temperature obtained from the energy balance of Equations (V.103) and (V.104). Equation (V.84) is modified to account for this enhanced mixing by

$$\frac{d}{dx} \left(\rho_L u_{EFF} H_{EFF} \right) = \frac{\rho_a kw(1 + \alpha)}{\phi(Ri'_*)} \tag{V.89}$$

where $Ri'_* = Ri_* \left(\frac{u_*}{w} \right)^2$.

Although derived for two-dimensional dispersion, this is extended for application to a denser-than-air gas plume which spreads laterally as a density intrusion:

$$\frac{d}{dx} \left(\rho_L u_{EFF} H_{EFF} B_{EFF} \right) = \frac{\rho_a kw(1 + \alpha)}{\phi(Ri'_*)} B_{EFF} \tag{V.90}$$

where the plume effective half width is defined by

$$B_{EFF} = b + \frac{\sqrt{\pi}}{2} S_y \tag{V.91}$$

and determined using the gravity intrusion relation

$$\frac{dB_{EFF}}{dt} = C_E \left[g \left(\frac{\rho - \rho_a}{\rho_a} \right) H_{EFF} \right]^{1/2} \tag{V.92}$$

The average transport velocity in the plume is defined by

$$u_{EFF} = \frac{\int_0^\infty cu_x dz}{\int_0^\infty cdz} = u_0 \left(\frac{S_z}{z_0} \right)^\alpha \Big/ \Gamma \left(\frac{1}{1+\alpha} \right) \qquad (V.93)$$

and the lateral spread of the cloud is modeled by

$$\frac{dB_{EFF}}{dx} = \frac{1}{u_{EFF}} \frac{dB_{EFF}}{dt}$$

$$= C_E \left[\frac{g z_0 \Gamma^3 \left(\frac{1}{1+\alpha} \right)}{u_0^2 (1+\alpha)} \right]^{1/2} \left[\frac{\rho - \rho_a}{\rho_a} \right]^{1/2} \left(\frac{S_z}{z_0} \right)^{\left(\frac{1}{2} - \alpha \right)} \qquad (V.94)$$

Horizontal Dispersion

The crosswind similarity parameter $S_y(x)$ is also determined by requiring that it satisfy the diffusion equation

$$u_x \frac{\partial c}{\partial x} = \frac{\partial}{\partial y} \left[K_y \frac{\partial c}{\partial y} \right] \qquad (V.95)$$

with the horizontal turbulent diffusivity given by

$$K_y = K_0 u_x B_{EFF}^{\gamma_1} \qquad (V.96)$$

When $b = 0$, $S_y = \sqrt{2}\,\sigma_y$, where σ_y is the similarity parameter correlated by Pasquill (1974) in the form $\sigma_y = \delta x^\beta$ where δ and β are functions of the Pasquill stability category and the averaging time. Furthermore, Equations (V.95) and (V.96) require that

$$\sigma_y \frac{d\sigma_y}{dx} = K_0 B_{EFF}^{\gamma_1} \qquad (V.97)$$

where $\gamma_1 = 2 - 1/\beta$ and $K_0 = \frac{2\beta}{\pi} (\delta\sqrt{\pi/2})^{1/\beta}$. Then,

$$S_y \frac{dS_y}{dx} = \frac{4\beta}{\pi} B_{EFF}^2 \left[\frac{\delta\sqrt{\pi/2}}{B_{EFF}} \right]^{1/\beta} \quad (V.98)$$

where Equation (V.98) is also assumed applicable for determining S_y when b is not zero.

At the downwind distance x_t where b = 0, the crosswind concentration profile is assumed Gaussian with S_y given by

$$S_y = \sqrt{2}\ \delta(x + x_v)^{\beta} \quad (V.99)$$

where x_v is a virtual source distance determined as

$$S_y(x_t) = \sqrt{2}\ \delta(x_t + x_v)^{\beta} \quad (V.100)$$

The gravity spreading calculation is terminated for $x > x_t$.

Although the effect of averaging time on the maximum downwind concentration for steady releases is still open to some question, the most important effect is assumed to be a result of plume meander for the purposes of the model. This behavior is reflected in the values of the dispersion parameters used in the Gaussian plume mode; Turner (1970) and Beals (1971) report different dispersion parameters for 10 minute average plume behavior and instantaneous or puff behavior. Because of plume meander, σ_y depends on the averaging time, while the value of σ_z is essentially unaffected by the averaging time (Beals, 1971). Therefore, the variation of σ_y is modeled as

$$\sigma_y(x;t_1)/\sigma_y(x;t_2) = (t_1/t_2)^p \quad (V.101)$$

where $\sigma_y(x;t_1)$ and $\sigma_y(x;t_2)$ are the values of σ_y associated with the averaging times t_1 and t_2, respectively. The value of p is a function of averaging time; Hino (1968) found p = 0.2 for averaging times less than 10 minutes and p = 0.5 for times greater than 10 minutes. Obviously, Equation (V.101) will not be appropriate as the averaging time goes to zero (i.e. for a puff). Using the values reported by Turner (1970), if the puff and 10 minute plume values of σ_y are compared for D stability, the equivalent averaging time for the puff coefficient is about 20 s. This result indicates that the width of a steady-state plume would not

vary significantly due to meander over any given 20 s period. (Note that the same statement would not be appropriate for the maximum concentration.) If the value of σ_y is parameterized as $\sigma_y = \delta x^{\beta}$ where σ_y and x are in meters, then the value of β can be approximated as being the same for the plume and puff values. (Seinfeld (1983) used $\beta = 0.894$ for the plume σ_y values.) Using the same power β, the parameterizations for plume and puff σ_y values are shown in Table V.2 where the averaging time for the puff coefficient is taken to be 20 s for all stabilities. For further discussion, see Spicer (1987) or Spicer and Havens (1987).

TABLE V.2
COEFFICIENT δ IN GAUSSIAN DISPERSION MODEL FOR USE IN $\sigma_y = \delta x^{\beta}$ WITH $\beta = 0.894$ AND σ_y AND x IN METERS

Averaging Time	Stability Class					
	A	B	C	D	E	F
10 min	0.443	0.324	0.216	0.141	0.105	0.071
20 s or less	0.224	0.164	0.109	0.071	0.053	0.036

For a steady plume, the centerline concentration c_c is determined from the material balance

$$E = \int_0^{\infty} \int_{-\infty}^{\infty} cu_x dydz = 2c_c \left(\frac{u_0 z_0}{1 + \alpha} \right) \left(\frac{S_z}{z_0} \right)^{1+\alpha} B_{EFF} \qquad (V.102)$$

where E is the plume source strength.

Energy Balance

For some simulations of cryogenic gas releases, heat transfer to the plume in the downwind dispersion calculation may be important, particularly in low wind conditions. The source calculation determines a gas/air mixture initial condition for the downwind dispersion problem. Air entrained into the plume is assumed to mix adiabatically. Heat transfer to the plume downwind of the source adds additional heat. This added heat per unit mass D_h is determined by an energy balance on a uniform cross-section as

$$\frac{d}{dx}\left[D_h \rho_L u_{EFF} H_{EFF} \right] = q_s/\delta_L \qquad (V.103)$$

where q_s is determined by Equation (V.37) along with the desired method of calculating h_0. Equation (V.103) is applied when b = 0 and is extended to

$$\frac{d}{dx}\left[D_h \rho_L u_{EFF} H_{EFF} B_{EFF} \right] = q_s B_{EFF}/\delta_L \qquad (V.104)$$

when b > 0. Since the average density of the layer ρ_L cannot be determined until the temperature (i.e. D_h) is known, a trial and error procedure is required.

Equations (V.77), (V.78), (V.79), (V.87)-(V.91), (V.94), and (V.98)-(V.104) are combined with an equation of state relating cloud density to gas concentration and temperature and are solved simultaneously to predict S_z, S_y, c_c, and b as functions of downwind distance beginning at the downwind edge of the gas source.

Correction for Along-Wind Dispersion

Following Colenbrander (1980), an adjustment to c_c is applied to account for dispersion parallel to the wind direction. The calculated centerline concentration $c_c(x)$ is considered to have resulted from the release of successive planar puffs of gas ($c_c(x)\Delta x$) without any dispersion in the x-direction. If it is assumed that each puff diffuses in the x-direction as the puff moves downwind independently of any other puff and that the dispersion is one-dimensional and Gaussian, the x-direction concentration dependence is given by

$$c_c'(x;x_{p_i}) = \frac{c_c(x_{p_i})\Delta x_i}{\sqrt{2\pi}\,\sigma_x} \exp\left[-\frac{1}{2}\left[\frac{x - x_{p_i}}{\sigma_x}\right]^2\right] \qquad \text{(V.105)}$$

where x_{p_i} denotes the position of the puff center due to observer i.

After Beals (1971), the x-direction dispersion coefficient σ_x is assumed to be a function of distance from the downwind edge of the gas source ($X = x - x_0$) and atmospheric stability given by

$$\begin{aligned} \sigma_x(X) &= 0.02\,X^{1.22} && \text{unstable, } x \geq 130 \text{ m} \\ &= 0.04\,X^{1.14} && \text{neutral, } x \geq 100 \text{ m} \\ &= 0.17\,X^{0.97} && \text{stable, } x \geq 50 \text{ m} \end{aligned} \qquad \text{(V.106)}$$

where ($X = x - x_0$) and σ_x are in meters. The concentration at x is then determined by superposition, i.e., the contribution to c_c at a given x from neighboring puffs is added to give an x-direction corrected value of c_c'. For N observers,

$$c_c'(x) = \sum_{i=1}^{N} \frac{c_c(x_{p_i})}{\sqrt{2\pi}\,\sigma_x} \exp\left[-\frac{1}{2}\left[\frac{x - x_{p_i}}{\sigma_x}\right]^2\right] \Delta x_i \qquad \text{(V.107)}$$

and for large N,

$$c_c'(x) = \frac{1}{\sqrt{2\pi}} \int_0^{\infty} \frac{c_c(\xi)}{\sigma_x(\xi - \xi_0)} \exp\left[-\frac{1}{2}\left[\frac{x - \xi}{\sigma_x(\xi - \xi_0)}\right]^2\right] d\xi \qquad \text{(V.108)}$$

The corrected centerline concentration c_c' is used in the assumed profiles in place of c_c, along with the distribution parameters S_y, S_z, and b.

VI. INTERFACING THE OOMS AND DEGADIS MODELS

The Ooms model presented here is intended to be used to predict the trajectory and dilution, to the point of (downwind) ground contact, of a dense gas jet released vertically upward into the atmospheric surface layer. The Ooms model prediction is terminated when the lower edge of the plume impinges the ground. The resulting downwind distance, plume centerline concentration and temperature, and plume radius ($\sqrt{2}b_j$) are used as input to DEGADIS. The ground level gas source input to DEGADIS is a circular area source with radius $\sqrt{2}b_j$ and concentration and temperature equal to the centerline values output from the Ooms model.

Application of the Ooms model to prediction of the trajectory and dilution of a dense gas jet, with subsequent input to DEGADIS for prediction of the ensuing ground level dispersion, is straightforward when the plume falls to the ground within a short distance downwind of the release point. If the plume remains aloft (because atmospheric entrainment results in dilution of the plume to an essentially passive state), it will continue to entrain air and grow in (circular) cross-section until the lower edge of the plume impinges the ground. For releases at elevations of a few meters (typical of chemical storage vessel vents), particularly under conditions of high atmospheric turbulence entrainment, the lower edge of the plume may impinge the ground at a short distance downwind. Since the plume centerline is still aloft it is questionable to input the resulting Ooms model output to DEGADIS (which assumes a ground level, area source). For this reason it is recommended that the jet release be simulated initially with the Ooms model to determine if the plume falls to the ground or remains aloft. If the plume centerline would fall to the ground within a short distance (say 1 kilometer) of the release point, the Ooms model output should be input to the DEGADIS model for prediction of the ensuing ground level dispersion. If the plume is predicted to remain aloft, the use of DEGADIS is not presently recommended, since the Ooms model does

not account for ground reflection of the plume and the "matching" of the Ooms output to a ground level gas source required by DEGADIS is not straightforward.

VII. CONCLUSIONS AND RECOMMENDATIONS

A mathematical model was developed for estimating ambient air concentrations downwind of elevated, denser-than-air gas jet-type releases. Ooms' model is used to predict the trajectory and dilution, to ground contact, of a denser-than-air jet/plume. The output of Ooms' model interfaces with the DEGADIS dense gas dispersion model to predict the ensuing ground level dispersion. The model incorporates momentum and heat transfer important to turbulent diffusion in the surface layer of the atmospheric boundary layer, and provides for:

- inputting data directly from external files
- treatment of ground-level or elevated sources
- estimation of maximum concentrations at fixed sites
- iteration over discrete meteorological conditions
- estimation of concentration-time history at fixed sites.

This report and the accompanying User's Guide (Volume II):

- document the theoretical basis of the model
- discuss its applicability and limitations
- discuss criteria for estimating the importance of gas density effects on a jet release from an elevated source
- define and describe all input variables and provide appropriate guidance for their specification
- identify and describe all output files and provide appropriate guidance for their interpretation
- provide user instructions for executing the code
- illustrate the model usage with example applications.

Application of the Ooms model to prediction of the trajectory and dilution of a dense gas jet, with subsequent input to DEGADIS for prediction of the ensuing ground level dispersion, is straightforward when the plume falls to the ground within a short distance downwind of the release point. If the plume remains aloft, it will continue to entrain air and grow in (circular) cross-section until the lower edge of the plume impinges the ground. For releases at elevations of a few

meters, the lower edge of the plume may impinge the ground at a short distance downwind. For jet/plumes which remain aloft, it is questionable to input the resulting Ooms model output to DEGADIS (which presently assumes a ground level, area source). Consequently, it is recommended that a jet release be simulated initially with the Ooms model to determine if the plume falls to the ground. If the plume (centerline) returns to the ground within a short distance (say 1 kilometer) of the release point, the Ooms model output can be input to the DEGADIS model for prediction of the ensuing ground level dispersion. If the plume is predicted to remain aloft, the use of DEGADIS is not presently recommended since the Ooms model does not account for ground reflection of the plume and the "matching" of the Ooms output to a ground level gas source required by DEGADIS is not straightforward.

The Ooms model is strictly applicable to steady state. However, in the intended application to denser-than-air jets, it is used to simulate the development of a jet-plume which would be time-limited (for example, a jet release of duration 5 minutes). The output of the jet model then provides a time-limited gas source for DEGADIS, which predicts the resulting (transient) downwind gas concentration history. Interfacing the Ooms model with DEGADIS for such applications can be problematical, particularly when the plume (gas-air) output of Ooms is very near ambient density. Although resolution of such difficulties appears to be relatively straightforward, time constraints in this effort were prohibitive. Additional work should be undertaken to resolve these difficulties, with the specific tasks:

- provide for "matching" of the Ooms model output mass flux rate with the DEGADIS atmospheric takeup at the Ooms-DEGADIS interface
- modify the Ooms model atmospheric turbulence entrainment specification to provide an elliptical cross-section and insure that the entrainment so specified is consistent with the Gaussian (Pasquill-Gifford) dispersion coefficient representation of atmospheric turbulence entrainment.

Address of these two (related) tasks would provide extension of the applicability of the model to description of plumes which become neutrally (or positively) buoyant.

REFERENCES

Albertson M. L., Y. B. Dai, R. A. Jenson, and H. Rouse, "Diffusion of Submerged Jets," Transactions of American Society of Civil Engineers, 115, (1950).

Batchelor, G. K., An Introduction to Fluid Dynamics, Cambridge University Press, Cambridge, UK, 1967.

Beals, G. A., "A Guide to Local Dispersion of Air Pollutants," Air Weather Service Technical Report 214, April, 1971.

Bird, R. B., W. E. Stewart, and E. N. Lightfoot, Transport Phenomena, John Wiley and Sons, New York, 1960.

Briggs, G. A., "Plume Rise," AEC Critical Review Series, USAEC Division of Technical Information Extension, Oak Ridge, Tennessee, 1969.

Britter, R. E., "The Ground Level Extent of a Negatively Buoyant Plume in a Turbulent Boundary Layer," Atmospheric Environment, 14, 1980.

Britter, R. E., unpublished monograph, 1980.

Businger, J. A., J. C. Wyngaard, Y. Izumi, and E. F. Bradley, "Flux-Profile Relationships in the Atmospheric Surface Layer," Journal of the Atmospheric Sciences, 28, March 1971.

Carnahan, B., H. A. Luther, and J. O. Wilkes, Applied Numerical Methods, John Wiley and Sons, 1969.

Colenbrander, G. W., "A Mathematical Model for the Transient Behavior of Dense Vapor Clouds," 3rd International Symposium on Loss Prevention and Safety Promotion in the Process Industries, Basel, Switzerland, 1980.

Colenbrander, G. W. and J. S. Puttock, "Dense Gas Dispersion Behavior: Experimental Observations and Model Developments," International Symposium on Loss Prevention and Safety Promotion in the Process Industries, Harrogate, England, September 1983.

Cude, II. L., "Dispersion of Gases Vented to Atmosphere from Relief Valves," The Chemical Engineer, October, 1974.

Havens, J. A. and T. O. Spicer, "Development of an Atmospheric Dispersion Model for Heavier-than-Air Gas Mixtures," Final Report to U.S. Coast Guard, CG-D-23-85, USCG HQ, Washington, DC, May 1985.

Hoot, T. G., R. N. Meroney, and J. A. Peterka, "Wind Tunnel Tests of Negatively Buoyant Plumes," Report CER73-74TGH-RNM-JAP-13, Fluid Dynamics and Diffusion Laboratory, Colorado State University, October 1973.

Hino, Mikio, "Maximum Ground-Level Concentration and Sampling Time," Atmospheric Environment, 2, pp. 149-165, 1968.

Kaimal, J. C., J. C. Wyngaard, D. A. Haugen, O. R. Cote, and Y. Izumi, "Turbulence Structure in the Convective Boundary Layer," J. Atmos. Sci., 33, 1976.

Kamotani, Yasuhiro and Isaac Greber, "Experiments on a Turbulent Jet in a Cross Flow," AIAA Journal, Vol. 10, No. 11, November 1972.

Kantha, H. L., O. M. Phillips, and R. S. Azad, "On Turbulent Entrainment at a Stable Density Interface," Journal of Fluid Mechanics, 79, 1977, pp. 753-768.

Koopman, R. P. et al., "Description and Analysis of Burro Series 40-m^3 LNG Spill Experiments," Lawrence Livermore National Laboratories Report UCRL-53186, August 14, 1981.

Lofquist, Karl, "Flow and Stress Near an Interface Between Stratified Liquids," Physics of Fluids, 3, No. 2, March-April 1960.

McAdams, W. H., Heat Transmission, McGraw-Hill, New York, 1954.

McQuaid, James, "Some Experiments on the Structure of Stably Stratified Shear Flows," Technical Paper P21, Safety in Mines Research Establishment, Sheffield, UK, 1976.

Morrow, T., "Analytical and Experimental Study to Improve Computer Models for Mixing and Dilution of Soluble Hazardous Chemicals," Final Report, Contract DOT-CG-920622-A with Southwest Research Institute, U.S. Coast Guard, August 1982.

Ooms, G., A. P. Mahieu, and F. Zelis, "The Plume Path of Vent Gases Heavier than Air," First International Symposium on Loss Prevention and Safety Promotion in the Process Industries, (C. H. Buschman, Editor), Elsevier Press, 1974.

Pasquill, F., Atmospheric Diffusion, 2nd edition, Halstead Press, New York, 1974.

Richards, J. M., "Experiments on the Motion of an Isolated Cylindrical Thermal Through Unstratified Surroundings," International Journal of Air and Water Pollution, 7, 1963.

Seinfeld, J. H., "Atmospheric Diffusion Theory," Advances in Chemical Engineering, 12, pp. 209-299, 1983.

Simpson, J. E. and R. E. Britter, "The Dynamics of the Head of a Gravity Current Advancing over a Horizontal Surface," Journal of Fluid Mechanics, 94, Part 3, 1979.

Spicer, T. O., "Using Different Time-Averaging Periods in DEGADIS," Report to the Exxon Education Foundation, June 1987.

Spicer, T. O. and J. A. Havens, "Development of Vapor Dispersion Models for Non-Neutrally Buoyant Gas Mixtures--Analysis of USAF/N_2O_4 Test Data," USAF Engineering and Services Laboratory, Draft Final Report, February, 1986.

Spicer, T. O. and J. A. Havens, "Development of Vapor Dispersion Models for Nonneutrally Buoyant Gas Mixtures--Analysis of TFI/NH_3 Test Data," UASF Engineering and Services Laboratory, Draft Final Report, July 1987.

Treybal, R. E., Mass Transfer Operations, 3rd edition, McGraw-Hill, New York, 1980.

Turner, D. B., "Workbook of Atmospheric Dispersion Estimates," USEPA 999-AP-26, U.S. Environmental Protection Agency, Washington DC, 1970.

van Ulden, A. P., "The Unsteady Gravity Spread of a Dense Cloud in a Calm Environment," 10th International Technical Meeting on Air Pollution Modeling and its Applications, NATO-CCMS, Rome, Italy, October 1979.

van Ulden, A. P., "A New Bulk Model for Dense Gas Dispersion: Two-Dimensional Spread in Still Air," I.U.T.A.M. Symposium on Atmospheric Dispersion of Heavy Gases and Small Particles, Delft University of Technology, The Netherlands, August 29-September 2, 1983.

Wheatley, C. J., "Discharge of Ammonia to Moist Atmospheres--Survey of Experimental Data and Model for Estimating Initial Conditions for Dispersion Calculations," UK Atomic Energy Authority Report SRD R410, 1986.

Zeman, O. and H. Tennekes, "Parameterization of the Turbulent Energy Budget at the Top of the Daytime Atmospheric Boundary Layer," Journal of the Atmospheric Sciences, January 1977.

TECHNICAL REPORT DATA
(Please read Instructions on the reverse before completing)

1. REPORT NO. EPA 450/4-88-006a	2.	3. RECIPIENT'S ACCESSION NO.
4. TITLE AND SUBTITLE A Dispersion Model for Elevated Dense Gas Jet Chemical Releases--Volume I		5. REPORT DATE April 1988 6. PERFORMING ORGANIZATION CODE
7. AUTHOR(S) Dr. Jerry Havens		8. PERFORMING ORGANIZATION REPORT NO.
9. PERFORMING ORGANIZATION NAME AND ADDRESS		10. PROGRAM ELEMENT NO. 11. CONTRACT/GRANT NO. P.O. #6D2746NASA
12. SPONSORING AGENCY NAME AND ADDRESS U.S. Environmental Protection Agency Office of Air Quality Planning and Standards Source Receptor Analysis Branch Research Triangle Park, N.C. 27711		13. TYPE OF REPORT AND PERIOD COVERED 14. SPONSORING AGENCY CODE

15. SUPPLEMENTARY NOTES

EPA Project Officer: Dave Guinnup

16. ABSTRACT

This document is the first of two volumes describing the development and use of a computer program designed to model the dispersion of heavier-than-air gases which are emitted into the atmosphere with significant velocity through elevated ports. The program incorporates the sequential execution of two models. The first one (Ooms) calculates the trajectory and dispersion of the gas plume as it falls to the ground. The second (DEGADIS) calculates the downwind dispersion after the plume touches ground.

This first volume discusses the development of both models and establishes the mathematical framework for the calculations. In addition, the trajectory portion of the model is evaluated in reference to wind tunnel data.

17. KEY WORDS AND DOCUMENT ANALYSIS

a. DESCRIPTORS	b. IDENTIFIERS/OPEN ENDED TERMS	c. COSATI Field/Group
Air pollution Dense gas Mathematical model Computer model	Dispersion Elevated sources	

18. DISTRIBUTION STATEMENT	19. SECURITY CLASS *(This Report)*	21. NO. OF PAGES
Release unlimited	88	
	20. SECURITY CLASS *(This page)*	22. PRICE

EPA Form 2220-1 (Rev. 4-77) PREVIOUS EDITION IS OBSOLETE